Control of Rotary Cranes Using Fuzzy Logic and Time-Delayed Position Feedback Control

Amjed A. Al-Mousa

Thesis submitted to the Faculty of the
Virginia Polytechnic Institute and State University
in partial fulfillment of the requirements for the degree of

Master of Science
in
Electrical Engineering

Ali Nayfeh, Co-Chair
Pushkin Kachroo, Co-Chair
Tim Pratt

November 27, 2000
Blacksburg, Virginia

Keywords: Tower Crane, Gantry Crane, Crane Control, Hybrid Control

Control of Rotary Cranes Using Fuzzy Logic and Time-Delayed Position Feedback Control

Amjed A. Al-Mousa

(ABSTRACT)

Rotary Cranes (Tower Cranes) are common industrial structures that are used in building construction, factories, and harbors. These cranes are usually operated manually. With the size of these cranes becoming larger and the motion expected to be faster, the process of controlling them became difficult without using automatic control methods. In general, the movement of cranes has no prescribed path. Cranes have to be run under different operating conditions, which makes closed-loop control preferable.

In this work, two types of controllers are studied: fuzzy logic and time-delayed position feedback controllers. The fuzzy logic controller is introduced first with the idea of split-horizon; that is, to use some fuzzy engines for tracking position and others for damping load oscillations. Then the time-delayed position feedback method is applied. Finally, an attempt to combine these two controllers into a hybrid controller is introduced. Computer simulations are used to verify the performance of these controllers. An experimental setup was built on which the time-delayed position feedback controller was tested. The results showed good performance.

This work was supported by the Office of Naval Research under Contract #N00014-96-1-1123.

To my Family

Acknowledgments

There are many people who have helped me a lot through out this work. First, I would like to thank Dr. Ali Nayfeh for his support, understanding, and the knowledge that I have gained while working with such a distinguished professor. Truly, it was a life time chance for me to work with Dr. Nayfeh. I would like also to thank Dr. Pushkin Kachroo for guiding me during this thesis and for the enthusiasm that I always had after meeting him. Dr. Tim Pratt also has contributed much to my engineering experience by passing to me the great engineering sense he has.

I would like to thank all of my colleagues in the Nonlinear Dynamics and Vibration Research Group, especially Ziyad Masoud. I have spend lots of my time through the last year working with Ziyad who provided me with endless help and advice. He saved no effort answering a question that I had, or correcting a mistake I have done. I can say nothing but that he was my helping hand and my real-time advisor. I would like to express my thanks also to Drs. Eihab Abdel Rahman and Haider Arafat for their help in introducing me to the world of nonlinear dynamics.

Finally, I would like to thank all of my friends who made the last year and a half really nice and stood beside me when I needed them.

Contents

List of Figures

List of Tables

Chapter 1

Introduction to Cranes

1.1 Cranes in Industry

The crane can be considered as one of the most important tools used in industry to transfer loads and cargo from one spot to another. Usually cranes have very strong structures in order to lift heavy payloads in factories, in building construction, on ships, and in harbors. In factories, cranes speed up the production processes by moving heavy materials to and from the factory as well as moving the products along production or assembly lines. In building construction, cranes facilitate the transport of building materials to high and critical spots. Similarly on ships and in harbors, cranes save time and consequently money in making the process of loading and unloading ships fast and efficient. Until recently, cranes were manually operated. But when cranes became larger and they are being moved at high speeds, their manual operation became difficult. Consequently, methods of automating their operation are being sought.

Figure 1.1: Gantry crane [17].

1.2 Types of Cranes

Cranes can be classified in terms of their mechanical structures and dynamics into three types: gantry, rotary, and boom cranes.

Gantry cranes (Figure 1.1) are characterized by a trolley moving over a jib (girder), the trolley motion can be described with a one-degree-of-freedom model. In some cases, the jib is mounted on another set of orthogonal railings in what is called bridge cranes. In this case, the trolley can move in a two-dimensional horizontal plane. They are common in factories because of their low cost, ease of assembly, and maintenance. They are also used in mines, steel-mill productions lines, and transport industry.

A rotary crane (Figure 1.2) consists of a jib that rotates in a horizontal plane around a fixed vertical axis. The trolley that holds the load can move radially over the jib. Hence, the combined motion of the trolley and jib can place the load at any point in the horizontal plane within the reach of the crane. The load is attached to the trolley using a set of cables.

Figure 1.2: Rotary crane [18].

Boom cranes (Figure 1.3) are very common on ships and in harbors. In general, a boom crane consists of a rotating base to which a boom is attached. The load hangs from the tip of the boom by a set of cables and pulleys. The rotational movement of the base along with the luff movement of the boom places the boom tip over any point in the horizontal plane, that is in reach of the crane. Meanwhile, changing the elevation (luff) angle of the boom causes a change in the radial and vertical positions of the load. The structure of boom cranes supports loads in compression, whereas rotary and gantry cranes support loads in a bending fashion. This makes boom cranes more compact than rotary and gantry cranes of similar capacities. Boom cranes are mounted on ships to transfer cargo between ships or on harbor pavements to transfer cargo between ships and offshore structures.

Figure 1.3: Boom cranes.

1.3 Literature Review

Several researchers have investigated the control of rotary cranes. Next, we summerize some of this recent work. Parker et al. [10, 11]presented several input shaping techniques to bring the load to rest at the end point of a predefined motion profile. However, up to 10° oscillations developed during maneuvers for given profiles. Parker et al. [12] presented another controller based on filtering the input signal commanded by the operator. The controller used a notch filter to eliminate the components of the slew and travel inputs that happen to be at the natural frequency of the payload pendulum. Even though experimental results showed reduced load pendulations through out the travel, a delay of up to 2.5 seconds occured between the operator input and the actual input from the filter to the cranes. This delay produces inconvenience to the operator. It could also cause confusion in case of accidental inputs. Also, because the notch filter is dependent on the length of the hoisting cable, the roll off factor of the filter had to be computed each time the cable length is changed.

Furthermore, the input shaping and the notch filter controllers are open-loop controllers, which make them inefficient in the presence of external disturbances.

As an example of closed-loop controllers, Golafshani et al. [9] generated time optimal trajectories of the jib, the trolley, and the cable length. A bang-bang controller was then used to track these optimal trajectories. Computer simulations showed uncontrolled load pendulations. To attain better results, they relaxed the constraint on time to 110% of the optimal value and obtained reduction in the payload pendulations. But still, significant pendulations persisted through out the maneuver.

Although the following discussion is directed at other types of cranes, it is useful and relevant to the design of controllers.

Nalley and Trabia [8] applied a distributed fuzzy logic controller to a bidirectional gantry crane. They introduced the idea of using two separate fuzzy controllers each of which has two fuzzy inference engines: one to track the desired position commanded by the operator and another to correct for payload oscillations. After performing all of the required calculations, the outputs of the two engines are combined to obtain the final control signal.The controller was used to drive the crane along a path generated by an input-shaping strategy. They obtained good results for damping the oscillations and at the same time reducing the payload travel time.

Masoud et al. [6] developed a time-delayed position feedback controller. The controller targeted boom cranes with base excitations. The controller forces the suspension point of the payload to follow an operator commanded motion to which a correction is added. The correction consists of a time-delayed percentage of the payload motion relative to the suspension point. The controller showed fast maneuvering time and low load oscillations throughout and at the end of the maneuvers.

1.4 Objective

One of the current problems in industry is that cranes became larger and higher. So they need to be faster to achieve acceptable transfer times. Unfortunately, cranes with large structures that are moving at high speeds are associated with undesirable payload oscillations resulting from the system dynamics. The objective of this work is to find a proper control strategy to transfer loads using rotary cranes. The control strategy should take into account two main factors. First, the time needed to move the payload from the initial pick up point to the destination point must be minimized. Second, the oscillation of the payload must be reduced to prevent hazards for people and equipment in the work place.

Chapter 2

Mathematical Modeling

In this chapter, we give a complete description of the crane model, a derivation of the equations of motion, and the corresponding state-space model. To derive a set of equations of motion that model the system dynamics, we use the Lagrangian approach.

2.1 Model Description

A rotary crane consists of a trolley that moves radially along a rotating jib. The jib rotates in a horizontal plane. The combined movements of the jib and the trolley enable positioning of the trolley and consequently the load over any point in the work space. The variation in the length of the hoisting cable is important for picking up the load, putting it down, and moving it away from obstacles. It also can be used as a part of the control strategy.

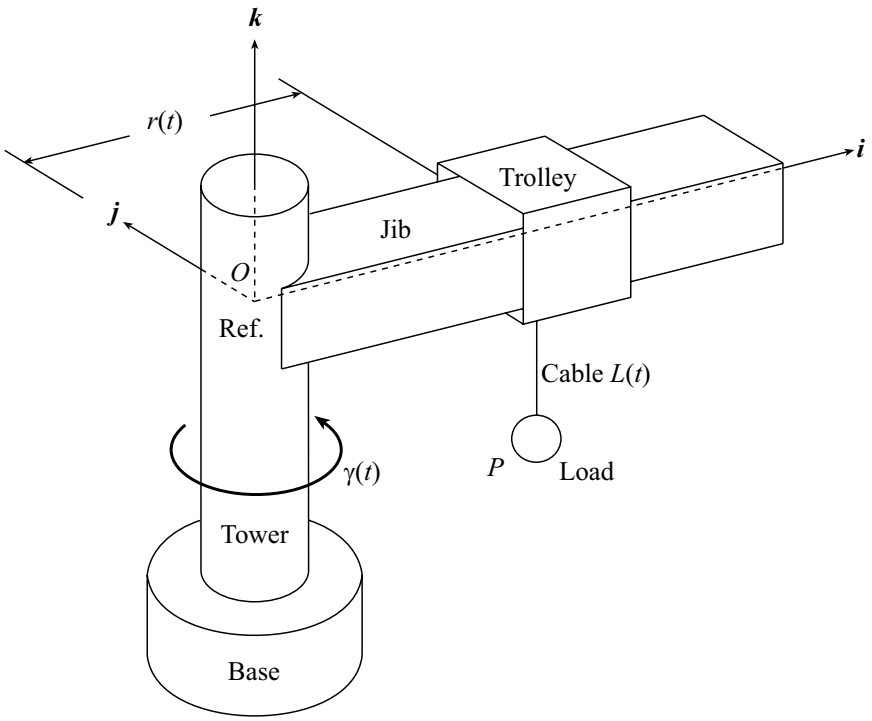

Figure 2.1: A 3D model of a rotary crane.

As shown in Figure 2.1, the structure of the crane consists of

(a) A tower that holds the jib of the crane; it is responsible for the rotational motion of the crane.

(b) A base that is usually fixed to the ground to prevent any oscillations.

(c) A jib that is mounted to the tower.

(d) A trolley that slides over the jib in a transverse direction.

(e) A suspension system of cables and pulleys. In the very general case, the length of the cable can be changed during load transport or at least at the pickup and end points. The process of changing the cable length is called hoisting.

2.2 System Parameters

To derive the equations of motion, one needs to define clearly the system parameters. As shown in Figure 2.1, a right-handed Cartesian coordinate system (xyz) is centered at a reference point that lies in the plane of the jib at the center of the crane tower, with its positive z-axis being along the tower upward axis. The $x-$ and $y-$axes are in the plane of the jib, with the x-axis being along the jib. The xyz coordinate system is attached to the moving jib. The jib rotates and traces an angle $\gamma(t)$. The trolley moves on the jib with its position $r(t)$ being the distance measured from the reference point of the xyz coordinate system to the suspension point of the payload cable on the trolley. The angle $\gamma(t)$ and the radial distance $r(t)$ are the inputs to the system. They are used to control the system behavior. We model the load as a point mass. The interaction between the load dynamics and the crane dynamics is neglected due to the assumption that the mass of the crane being very large compared to that of the load. We start by defining the velocity of the trolley in the jib-fixed coordinate system as

$$v_x = \dot{r}\mathbf{i} \tag{2.1}$$

and its acceleration

$$a_x = \ddot{r}\mathbf{i} \tag{2.2}$$

The angular velocity of the jib is

$$\omega = \dot{\gamma}\mathbf{k} \tag{2.3}$$

and its angular acceleration is

$$\alpha = \ddot{\gamma}\mathbf{k} \tag{2.4}$$

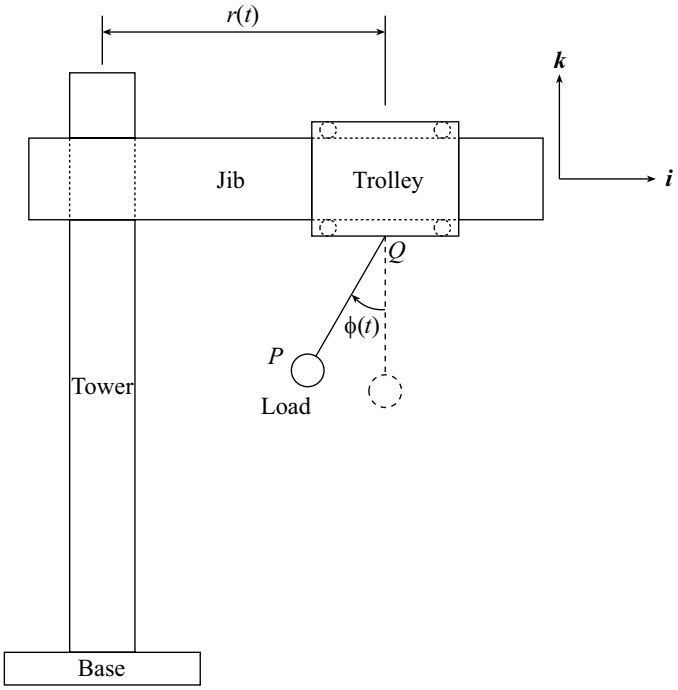

Figure 2.2: Side view of the crane showing the in-plane angle ϕ.

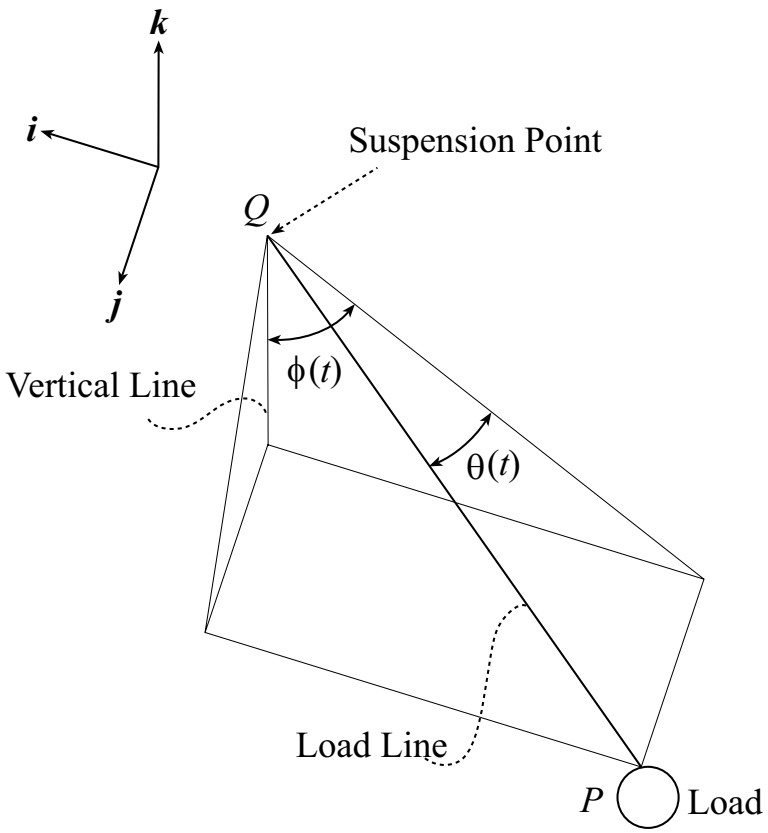

Figure 2.3: Oscillation angles $\phi(t)$ and $\theta(t)$ of the load.

The load pendulations are characterized by two angles, ϕ and θ. The angle ϕ is the angle which the cable makes with the z-axis in the xz-plane, a shown in Figure 2.2. The out-of-plane angle θ is the angle which the cable makes with the xz-plane. So it is clear now that the objective of the controller is to move the payload while keeping ϕ and θ as small as possible, Figure 2.3.

2.3 Derivation of the Equations of Motion

The first step in deriving the equations of motion using the Lagrangian approach is to find the position P(t) of the load with respect to the reference point O. In the jib-fixed coordinate system, the load position is

$$P(t) = [r(t) - L(t)\cos\theta(t)\sin\phi(t)]\mathbf{i} + [L(t)\sin\theta(t)]\mathbf{j} - [L(t)\cos\theta(t)\cos\phi(t)]\mathbf{k} \tag{2.5}$$

To determine the kinetic energy of the load, we need to determine the velocity $\dot{P}$(t) of the load. Since the jib is moving,

$$\dot{P}(t) = \frac{\partial P(t)}{\partial t} + \omega(t) \times P(t) \tag{2.6}$$

where

$$\omega(t) = \dot{\gamma}(t)\mathbf{k} \tag{2.7}$$

Hence, the absolute velocity of the payload is

$$\begin{aligned}\dot{P}(t) =&[\dot{r}(t) - \dot{L}(t)\sin\phi(t)\cos\theta(t) - L(t)(\dot{\gamma}(t)\sin\theta(t) \\ &- \dot{\theta}(t)\sin\theta(t)\sin\phi(t) + \dot{\phi}(t)\cos\theta(t)\cos\phi(t))]\mathbf{i} \\ &+ [\dot{L}(t)\sin\theta(t) + r(t)\dot{\gamma}(t) + L(t)\cos\theta(t)(\dot{\theta}(t) - \dot{\gamma}(t)\sin\phi(t))]\mathbf{j} \\ &+ [-\dot{L}(t)\cos\theta(t)\cos\phi(t) + L(t)(\dot{\theta}\sin\theta(t)\cos\phi(t) + \dot{\phi}(t)\sin\phi(t)\cos\theta(t))]\mathbf{k}\end{aligned} \tag{2.8}$$

The kinetic energy of the load is

$$K_E = \frac{1}{2} m_{Load} [\dot{P}(t).\dot{P}(t)] \tag{2.9}$$

or

$$\begin{aligned} K_E =& \frac{1}{2} m_{Load} \{ [\dot{L}(t)\sin\theta(t) + r(t)\dot{\gamma}(t) + L(t)\cos\theta(t)(\dot{\theta}(t) - \dot{\gamma}(t)\sin\theta(t))]^2 \\ &+ [\dot{r}(t) - \dot{L}(t)\sin\phi(t)\cos\theta(t) - L(t)(\dot{\gamma}(t)\sin\theta(t) - \dot{\theta}(t)\sin\theta(t)\sin\phi(t) \\ &+ \dot{\phi}(t)\cos\theta(t)\cos\phi(t))]^2 + [-\dot{L}(t)\cos\phi(t)\cos\theta(t) + L(t)(\dot{\theta}(t)\sin\theta(t)\cos\phi(t) \\ &+ \dot{\phi}(t)\cos\theta(t)\sin\phi(t))]^2 \} \end{aligned} \tag{2.10}$$

The potential energy of the payload is given by

$$P_E = -m_{Load} g L(t)\cos\theta(t)\cos\phi(t) \tag{2.11}$$

Finally, the Lagrangian $\mathcal{L}$ is given by

$$\mathcal{L} = K_E - P_E \tag{2.12}$$

or

$$\begin{aligned} \mathcal{L} =& \frac{1}{2} m_{Load} \{ 2gL(t)\cos\theta(t)\cos\phi(t) + [\dot{L}(t)\sin\theta(t) + r(t)\dot{\gamma}(t) \\ &+ L(t)\cos\theta(t)(\dot{\theta}(t) - \dot{\gamma}(t)\sin\theta(t))]^2 + [\dot{r}(t) - \dot{L}(t)\sin\phi(t)\cos\theta(t) \\ &- L(t)(\dot{\gamma}(t)\sin\theta(t) - \dot{\theta}(t)\sin\theta(t)\sin\phi(t) + \dot{\phi}(t)\cos\theta(t)\cos\phi(t))]^2 \\ &+ [-\dot{L}(t)\cos\phi(t)\cos\theta(t) + L(t)(\dot{\theta}(t)\sin\theta(t)\cos\phi(t) \\ &+ \dot{\phi}(t)\cos\theta(t)\sin\phi(t))]^2 \} \end{aligned} \tag{2.13}$$

The Euler Lagrange equations corresponding to $\mathcal{L}$ are

$$\frac{d}{dt}\left(\frac{\partial \mathcal{L}}{\partial x_i}\right) - \frac{\partial \mathcal{L}}{\partial x_i} = 0 \tag{2.14}$$

where $x_1 = \theta$ and $x_2 = \phi$. This will yield the following two nonlinear equations of motion:

$$\begin{aligned} & L(t)\ddot{\theta}(t) + 2\dot{L}(t)\dot{\theta}(t) - 2L(t)\dot{\gamma}(t)\cos\phi(t)\cos^2\theta(t)\dot{\phi}(t) + \frac{1}{2}L(t)\sin 2\theta(t)\dot{\phi}^2(t) \\ & - \frac{1}{2}L(t)\dot{\gamma}^2(t)\sin 2\theta(t)\cos^2\phi(t) + g\sin\theta(t)\cos\phi(t) + 2\dot{r}(t)\dot{\gamma}(t)\cos\theta(t) \\ & - r(t)\dot{\gamma}^2(t)\sin\phi(t)\sin\theta(t) + \ddot{r}(t)\sin\theta(t)\sin\phi(t) - 2\dot{L}(t)\dot{\gamma}(t)\sin\phi(t) \\ & + r(t)\ddot{\gamma}(t)\cos\theta(t) - L(t)\ddot{\gamma}(t)\sin\phi(t) = 0 \end{aligned} \tag{2.15}$$

and

$$\begin{aligned} & L(t)\cos\theta(t)\ddot{\phi}(t) + 2\dot{L}(t)\cos\theta(t)\dot{\phi}(t) + 2L(t)\dot{\gamma}(t)\cos\theta(t)\cos\phi(t)\dot{\theta}(t) \\ & - 2L(t)\sin\theta(t)\dot{\theta}(t)\dot{\phi}(t) + g\sin\phi(t) + 2\dot{L}(t)\dot{\gamma}(t)\cos\phi(t)\sin\theta(t) \\ & + \cos\phi(t)\dot{\gamma}^2(t)[r(t) - L(t)\sin\phi(t)\cos\theta(t)] + L(t)\ddot{\gamma}(t)\sin\theta(t)\cos\phi(t) \\ & - \ddot{r}(t)\cos\phi(t) = 0 \end{aligned} \tag{2.16}$$

For our case, the cable length $\mathsf{L(t)}$ is set equal to a constant value, then

$$\frac{dL}{dt} = 0 \tag{2.17}$$

Substituting equation (2.17) into equations (2.15) and (2.16) yields

$$\begin{aligned} & \ddot{\theta}(t) - 2\dot{\gamma}(t)\cos\phi(t)\cos^2\theta(t)\dot{\phi}(t) + \frac{1}{2}\sin 2\theta(t)\dot{\phi}^2(t) \\ & - \frac{1}{2}\dot{\gamma}^2(t)\sin 2\theta(t)\cos^2\phi(t) + \frac{g}{L}\sin\theta(t)\cos\phi(t) + \frac{2}{L}\dot{r}(t)\dot{\gamma}(t)\cos\theta(t) \\ & - \frac{1}{L}r(t)\dot{\gamma}^2(t)\sin\phi(t)\sin\theta(t) + \frac{1}{L}\ddot{r}(t)\sin\theta(t)\sin\phi(t) + \frac{1}{L}r(t)\ddot{\gamma}(t)\cos\theta(t) \\ & - \ddot{\gamma}(t)\sin\phi(t) = 0 \end{aligned} \tag{2.18}$$

and

$$\begin{aligned} & \cos\theta(t)\ddot{\phi}(t) + 2\dot{\gamma}(t)\cos\theta(t)\cos\phi(t)\dot{\theta}(t) - 2\sin\theta(t)\dot{\theta}(t)\dot{\phi}(t) \\ & + \frac{g}{L}\sin\phi(t) + \cos\phi(t)\dot{\gamma}^2(t)[\frac{r(t)}{L} - \sin\phi(t)\cos\theta(t)] \\ & + \ddot{\gamma}(t)\sin\theta(t)\cos\phi(t) - \frac{1}{L}\ddot{r}(t)\cos\phi(t) = 0 \end{aligned} \tag{2.19}$$

2.4 State-Space Model of the Crane

For easier manipulation of the crane parameters, we reformulate the equations of motion in state-space form. The following equations are used later to simulate the system dynamics. To this end, we let

$$x_1 = \theta(t) \tag{2.20}$$

$$x_2 = \phi(t) \tag{2.21}$$

$$x_3 = r(t) \tag{2.22}$$

$$x_4 = \gamma(t) \tag{2.23}$$

$$x_5 = \dot{\theta}(t) \tag{2.24}$$

$$x_6 = \dot{\phi}(t) \tag{2.25}$$

$$x_7 = \dot{r}(t) \tag{2.26}$$

$$x_8 = \dot{\gamma}(t) \tag{2.27}$$

$$U_1 = \ddot{r}(t) \tag{2.28}$$

$$U_2 = \ddot{\gamma}(t) \tag{2.29}$$

Hence,

$$\dot{x}_1 = x_5 \tag{2.30}$$

$$\dot{x}_2 = x_6 \tag{2.31}$$

$$\dot{x}_3 = x_7 \tag{2.32}$$

$$\dot{x}_4 = x_8 \tag{2.33}$$

$$\dot{x}_7 = U_1 = \ddot{r}(t) \tag{2.34}$$

$$\dot{x}_8 = U_2 = \ddot{\gamma}(t) \tag{2.35}$$

Then, it follows from equations (2.18) and (2.19) that

$$\begin{aligned}\dot{x}_5 = &-\frac{1}{2L}(2g\cos x_2 \sin x_1 + 4x_7 x_8 \cos x_1 - L{x_8}^2 \sin 2x_1 \cos^2 x_2 \\ &- 2x_3 {x_8}^2 \sin x_1 \sin x_2 - 4Lx_6 x_8 \cos x_2 \cos^2 x_1 + L{x_6}^2 \sin 2x_1 + 2\sin x_1 \sin x_2 U_1 \\ &+ 2x_3 \cos x_1 U_2 - 2L \sin x_2 U_2)\end{aligned} \tag{2.36}$$

$$\begin{aligned}\dot{x_6} = &-\frac{1}{L\cos x_1}(g\sin x_2 + x_3 {x_8}^2 \cos x_2 - L{x_8}^2 \sin x_2 \cos x_1 \cos x_2 \\ &+ 2Lx_5 x_8 \cos x_1 \cos x_2 - 2Lx_5 x_6 \sin x_1 - \cos x_2 U_1 + L\sin x_1 \cos x_2 U_2)\end{aligned} \tag{2.37}$$

Chapter 3

Fuzzy Logic Controller

Fuzzy logic is the first approach that we have tried to control the crane. An introduction to fuzzy control logic is first presented. A detailed description of the controller design is also introduced. Finally, simulation results of the controller are presented.

3.1 Introduction to Fuzzy Logic Control

Fuzzy logic is one of the recent developing methods in control that are gaining more popularity. The idea behind fuzzy logic is to write rules that will operate the controller in a heuristic manner, mainly in an (If A Then B) format. The arguments A and B are not exact numbers or equations, but they are descriptive words or phrases like small, pretty cold, and very high.

Any fuzzy controller consists of four main stages: variable fuzzification, rules application, aggregation, and defuzzification stages [1, 16]. These stages have many variations, so all the details mentioned later are specific to the design we have chosen.

Starting with the fuzzification stage, we map all of the crisp (numerical) values of the

input variable into memberships in fuzzy logic sets. The whole crisp range is mapped into a number of fuzzy logic sets. The degree of membership for a certain numerical input depends on the shape of the fuzzy set and where does the crisp value lie in the range of this set. For example, in Figure 3.1, the variable $\phi = 1.25$ has 0.75 membership in Positive Small (PS) and 0.25 in Positive Medium (PM), while it has zero membership in the other sets. The shape of the membership functions is chosen to be triangular.

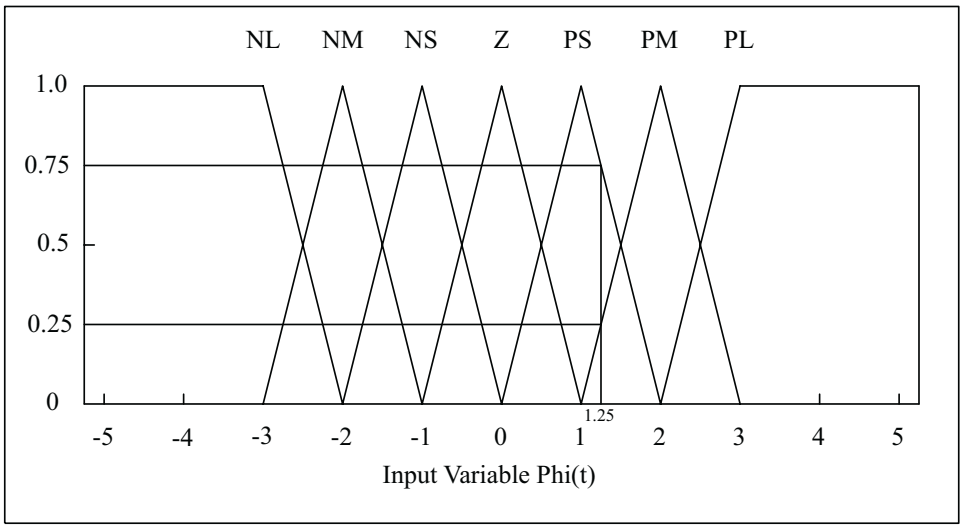

Figure 3.1: Example on fuzzy logic sets.

Then, we apply the rules one at a time. If the antecedents of the rule are combined by an AND operator, then the minimum of all of the antecedent memberships is taken to be the membership of the output. But if they are combined by an OR operator, then the maximum membership is taken to be the output membership.

After applying all of the fuzzy rules, the aggregation stage starts. At this stage, all of the outputs of the rules that belong to the same output variable are aggregated together. Summing all of the outputs is the method chosen for this controller.

Eventually, in the defuzzification stage, a crisp value is assigned for the output. Find-

ing the centroid of the output shape is the method used here [2].

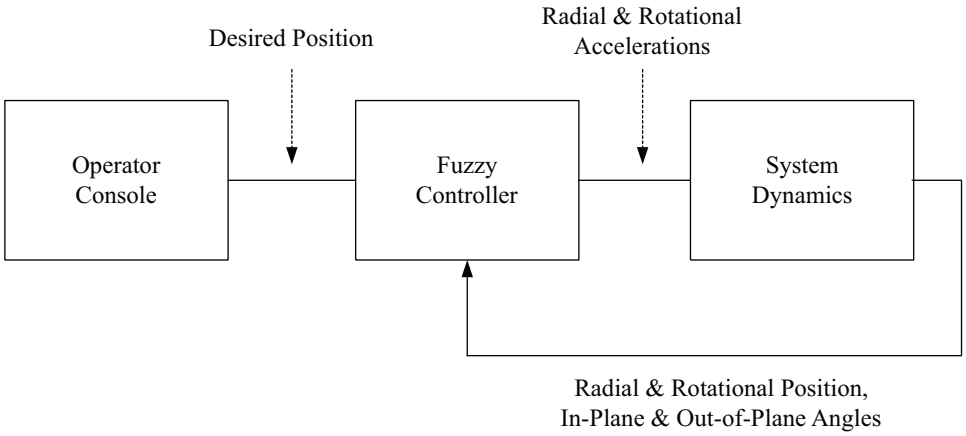

Figure 3.2: System block diagram with fuzzy logic controller.

3.2 Fuzzy Logic Controller Design

As shown in Figure 3.2, we start with the input signals from the operator. These signals represent the desired radial position $r_d(t)$ and rotational angle $\gamma_d(t)$. These two signals can be read from the operator's handle (joy stick). The fuzzy controller receives four other inputs from the feedback loop: the actual radial distance $r_a(t)$, the actual rotational angle $\gamma_a(t)$, the in-plane angle $\phi(t)$, and the out-of-plane angle $\theta(t)$. The fuzzy logic controller (FLC) generates the radial and rotational accelerations, which are inputs to the system dynamics block. From Figure 3.3, it is clear that two separate controllers are employed. One is radial, which takes care of the transverse motion of the trolley over the jib; and the other is rotational, which handles the rotational motion of the jib.

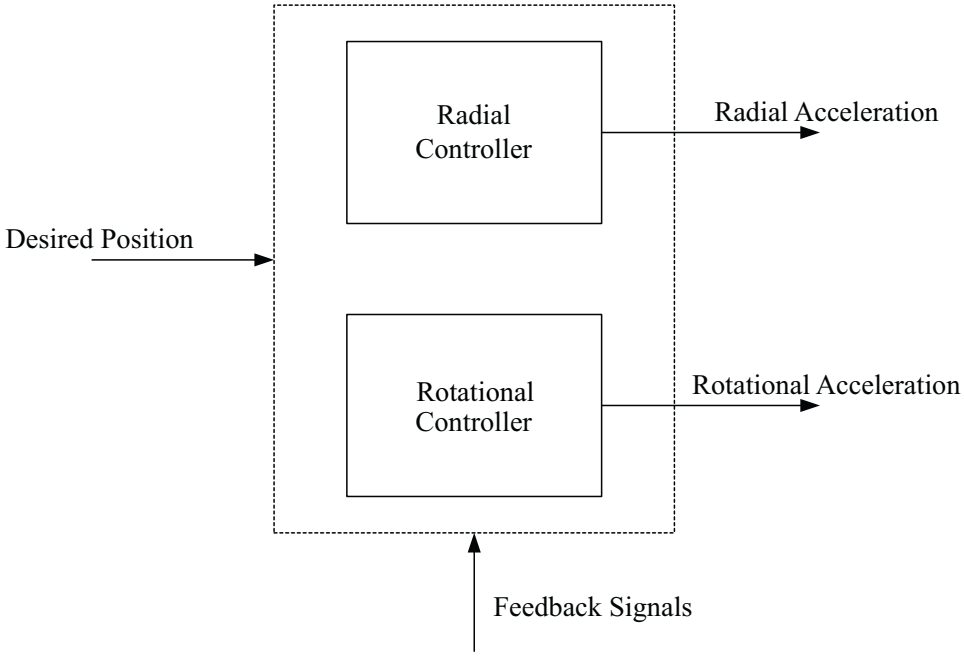

Figure 3.3: Fuzzy logic controller design.

Two fuzzy inference engines (FIE) are used inside each controller, Figure 3.4. The first is the tracking FIE, which has the desired and actual radial distances as inputs for the radial controller and the desired and actual rotational angles as inputs for the rotational controller. Meanwhile the oscillations damping FIE has the in-plane angle ϕ as an input for the radial controller and the out-of-plane angle θ as inputs for the rotational controller. The outputs of the two FIEs are inputs to a variable-share mixing block, where the output from the tracking FIE is multiplied by a factor K and the oscillations damping FIE output is multiplied by $1 - K$. Then, the scaled outputs are added to obtain the controller output (acceleration).

Through the design, the gain K is assigned a fixed value to obtain the optimal performance of the system. But it can be varied or it can be changed by the operator according to the current conditions of transportation. The output of the radial controller is $\ddot{r}_{Reference}(t)$, and the output of the rotational controller is $\ddot{\gamma}_{Reference}(t)$.

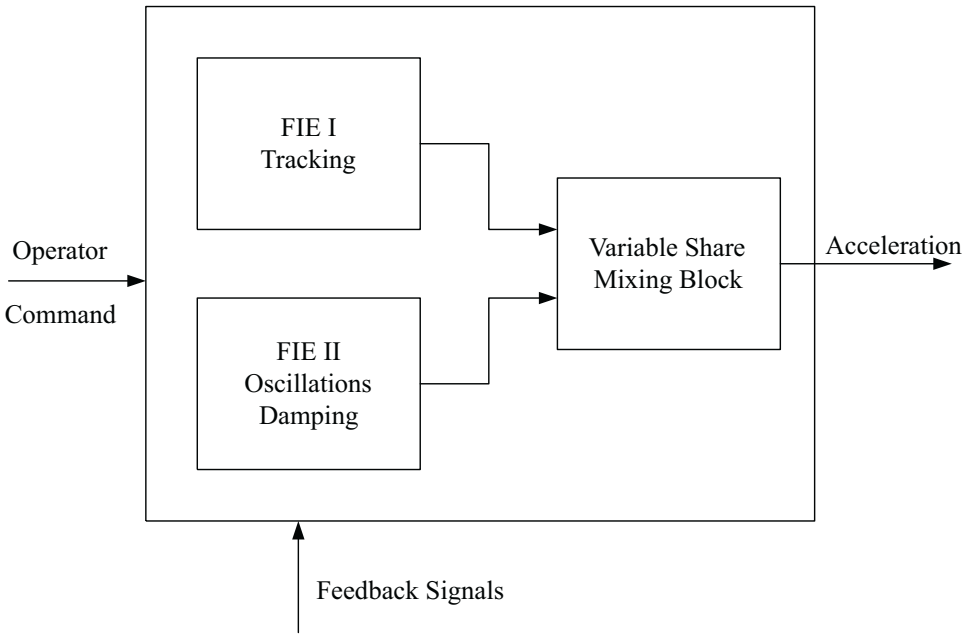

Figure 3.4: Two FIEs are inside each FLC.

Next, we describe each controller and explain the fuzzy sets and rules in each FIE.

3.2.1 Radial Controller

This controller determines the radial acceleration of the trolley, which is fed to the system dynamics block to find the response. The outputs of the following FIEs are mixed with a gain $K_{Radial} = 0.8$.

Tracking FIE

This FIE has the actual radial distance $r_a(t)$ and the desired radial distance $r_d(t)$ and their derivatives $\dot{r}_a(t)$ and $\dot{r}_d(t)$. Its output is $\ddot{r}_{Track}$. Before applying the fuzzy rules, we calculate

two variables, the radial distance error $E_r(t)$ and its derivative as follows:

$$E_r(t) = r_d(t) - r_a(t) \tag{3.1}$$

and

$$\dot{E}_r(t) = \dot{r}_d(t) - \dot{r}_a(t) \tag{3.2}$$

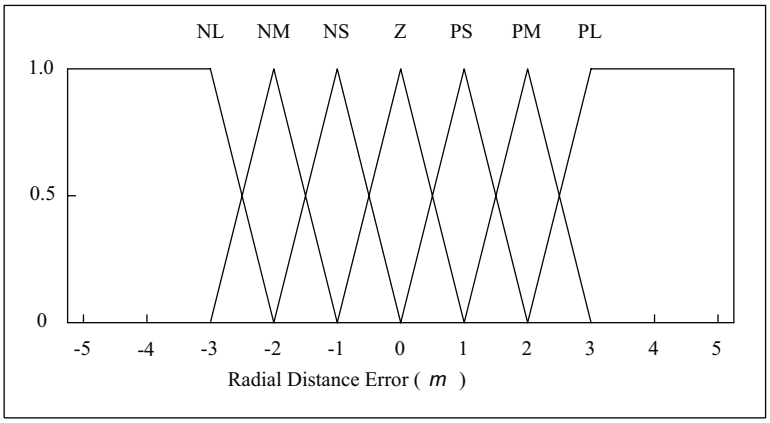

Figure 3.5: Fuzzification of $E_r(t)$.

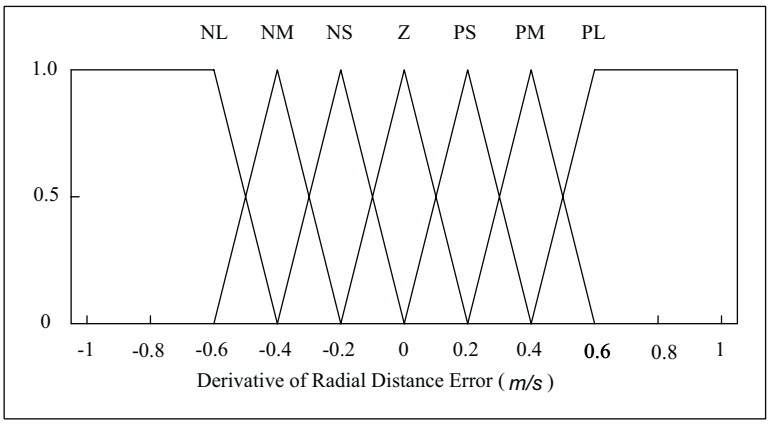

Figure 3.6: Fuzzification of $\dot{E}_r(t)$.

Then, they are fuzzified using the fuzzy sets shown in Figures 3.5 and 3.6, and subsequently the rules in Table 3.1 are applied in order to find $\ddot{r}_{Track}$[1].

Table 3.1: Rules for the radial tracking FIE.

		Derivative of Radial Distance Error						
		PL	PM	PS	Z	NS	NM	NL
	PL	PL	PL	PM	PM	PS	PS	Z
	PM	PL	PM	PM	PS	PS	Z	NS
Radial	PS	PM	PM	PS	PS	Z	NS	NS
Distance	Z	PM	PS	PS	Z	NS	NS	NM
Error	NS	PS	PS	Z	NS	NS	NM	NM
	NM	PS	Z	NS	NS	NM	NM	NL
	NL	Z	NS	NS	NM	NM	NL	NL

As a result of applying the previous rules, we have a fuzzy notion of the output variable $\ddot{r}_{Track}$, which is transformed into a crisp value using the centroid method. Figure 3.7 shows the fuzzy sets of $\ddot{r}_{Track}$.

Oscillations Damping FIE

In the oscillations damping FIE, the input variables are $\phi(t)$ and $\dot{\phi}(t)$. The rules here are based on imitating a quarter-period delay controller. It tries to position the trolly over the load in order to damp any oscillations. The inputs to the FIE are fuzzified using the fuzzy sets shown in Figures 3.8 and 3.9. Similarly, the fuzzy rules in Table 3.2 are now applied to find the $\ddot{r}_{Correction}$. After applying the rules, again we resort to defuzzify the output in order

[1] These are generic fuzzy PD controller rules, the one's used here are similar to those used by Nally and Trabia [8].

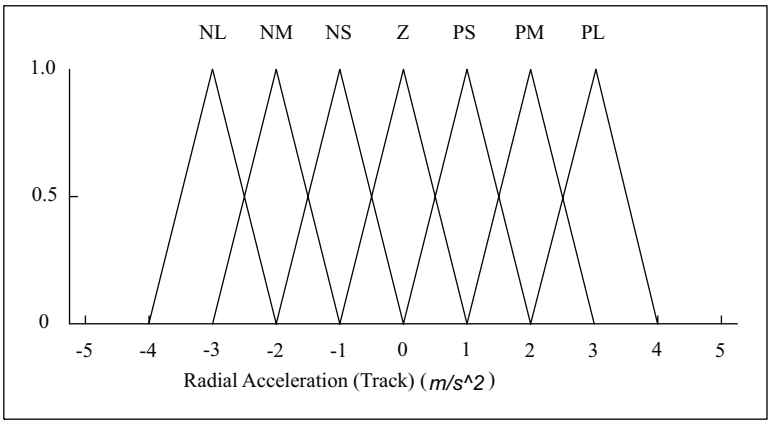

Figure 3.7: Defuzzification of $\ddot{r}_{Track}$.

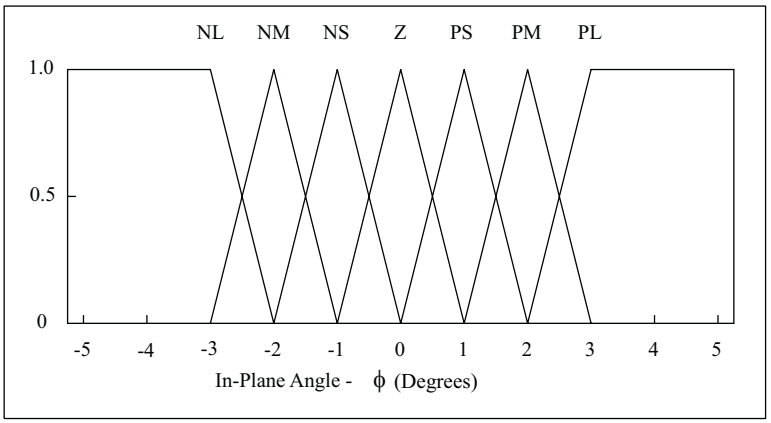

Figure 3.8: Fuzzification of $\phi(t)$.

Table 3.2: Rules for the radial oscillations damping FIE.

		In-plane angle ϕ(t)						
		PL	PM	PS	Z	NS	NM	NL
Derivative	P	NL	NM	NS	Z	PS	PM	PL
of in-plane	Z	Z	Z	Z	Z	Z	Z	Z
angle $\dot{\phi}$(t)	N	NL	NM	NS	Z	PS	PM	PL

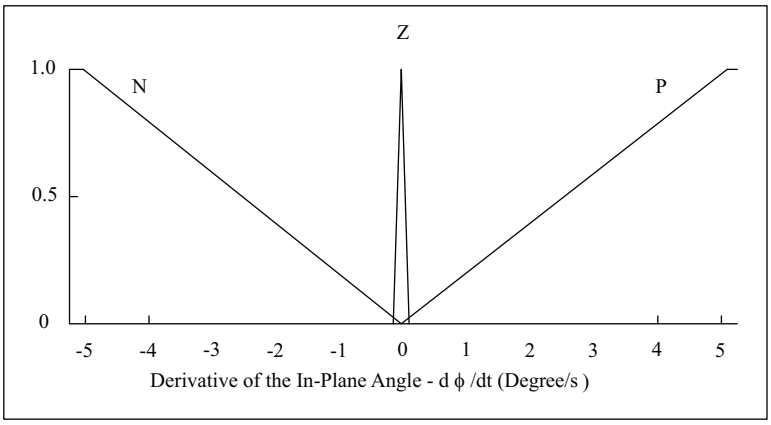

Figure 3.9: Fuzzification of $\dot{\phi}(t)$.

to find $\ddot{r}_{Correction}$. Figure 3.10 shows the fuzzy sets of $\ddot{r}_{Correction}$.

Now, the output of this controller can be found by

$$\ddot{r}_{Reference}(t) = 0.8 \times \ddot{r}_{Track} + 0.2 \times \ddot{r}_{Correction} \tag{3.3}$$

3.2.2 Rotational Controller

Similar to the radial controller, the rotational controller consists also of two FIEs. It was found that the optimal value for the mixing gain $K_{Rotational} = 0.6$. This lower value shows that it take more control action to damp the out-of-plane angle $\theta(t)$ than the in-plane angle $\phi(t)$, which is expected because any attempt to reduce any out-of-plane oscillations induces in-plane ones, thus causing more problems.

Tracking FIE

Here the FIE has the actual rotational angle $\gamma_a(t)$, the desired rotational angle $\gamma_d(t)$, and their derivatives $\dot{\gamma}_a(t)$ and $\dot{\gamma}_d(t)$. The FIE output is $\ddot{\gamma}_{Track}$. Before applying the fuzzy rules, we calculate two other variables, the rotational angle error $E_\gamma(t)$ and the derivative of the

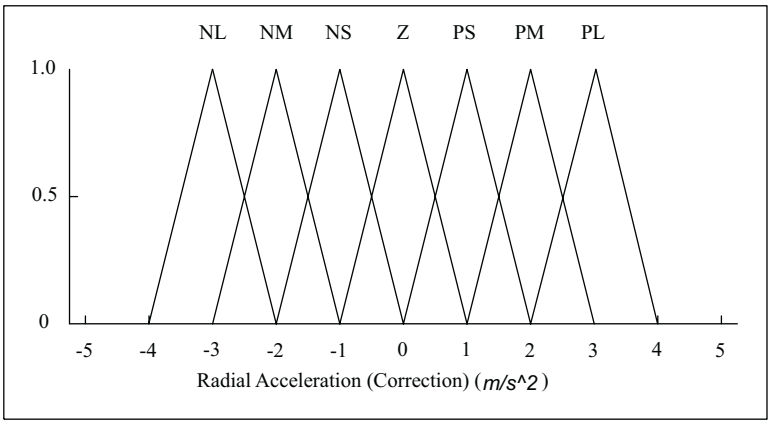

Figure 3.10: Defuzzification of $\ddot{r}_{Correction}$.

rotational angle error $\dot{E}_\gamma(t)$ as follows:

$$E_\gamma(t) = \gamma_d(t) - \gamma_a(t) \tag{3.4}$$

and

$$\dot{E}_\gamma(t) = \dot{\gamma}_d(t) - \dot{\gamma}_a(t) \tag{3.5}$$

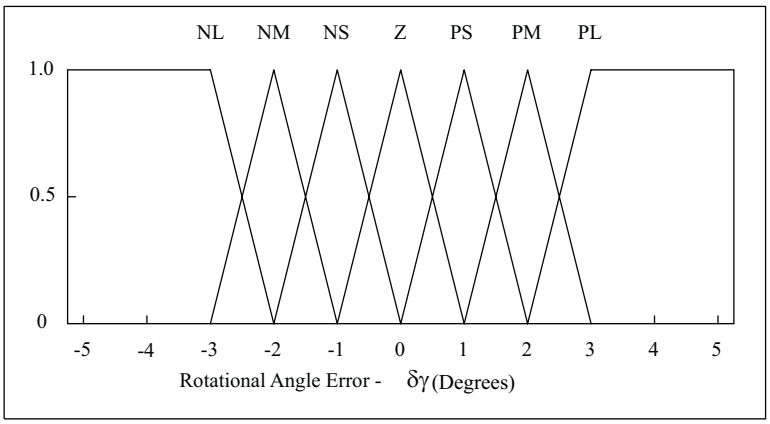

Figure 3.11: Fuzzification of $E_\gamma(t)$.

Then they are fuzzified using the fuzzy sets shown in Figures 3.11 and 3.12. After

that the rules in Table 3.3 are applied in order to find $\ddot{\gamma}_{Track}$[2].

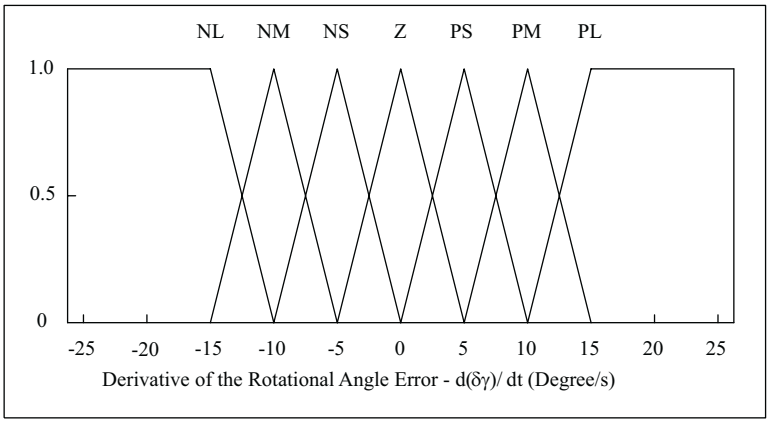

Figure 3.12: Fuzzification of $\dot{E}_{\gamma}(t)$.

Table 3.3: Rules for the rotational tracking FIE.

		Derivative of rotational angle error						
		PL	PM	PS	Z	NS	NM	NL
Rotational angle error	PL	PL	PL	PM	PM	PS	PS	Z
	PM	PL	PM	PM	PS	PS	Z	NS
	PS	PM	PM	PS	PS	Z	NS	NS
	Z	PM	PS	PS	Z	NS	NS	NM
	NS	PS	PS	Z	NS	NS	NM	NM
	NM	PS	Z	NS	NS	NM	NM	NL
	NL	Z	NS	NS	NM	NM	NL	NL

After applying the rules, we obtain the output variable $\ddot{\gamma}_{Track}$ in a fuzzy format, which is

[2] These are generic fuzzy PD controller rules, the one's used here are similar to those used by Nally and Trabia [8].

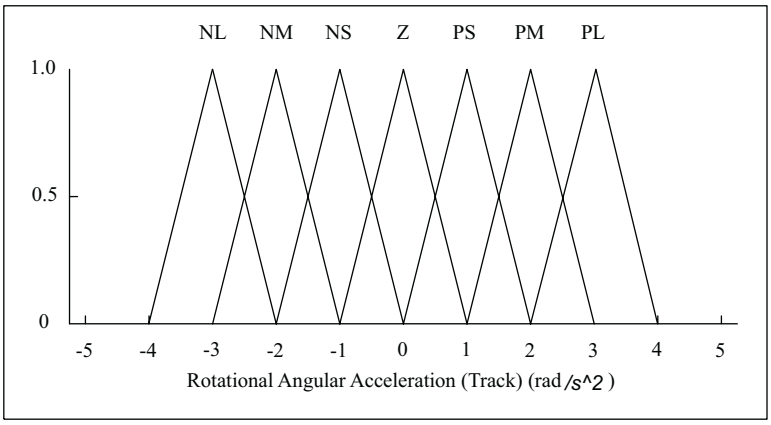

Figure 3.13: Defuzzification of $\ddot{\gamma}_{Track}$.

transformed into a crisp value using the centroid method also. Figure 3.13 shows the fuzzy sets of $\ddot{\gamma}_{Track}$.

Oscillations Damping FIE

For the oscillations damping FIE, the input variables are $\theta(t)$ and $\dot{\theta}(t)$. The rules here are based on the same concept used for the radial controller. The inputs to the FIE are fuzzified using the fuzzy sets shown in Figures 3.14 and 3.15. Again the fuzzy rules in Table 3.4 are now applied to find the $\ddot{\gamma}_{Correction}$.

Table 3.4: Rules for the rotational oscillations damping FIE.

		Out-of-plane angle ϕ(t)						
		PL	PM	PS	Z	NS	NM	NL
Derivative of	P	PL	PM	PS	Z	NS	NM	NL
out-of-plane	Z	Z	Z	Z	Z	Z	Z	Z
angle $\dot{\phi}$(t)	N	PL	PM	PS	Z	NS	NM	NL

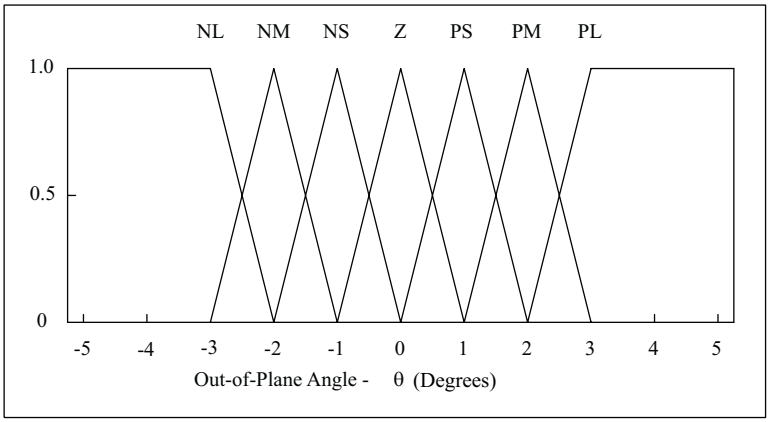

Figure 3.14: Fuzzification of $\theta(t)$.

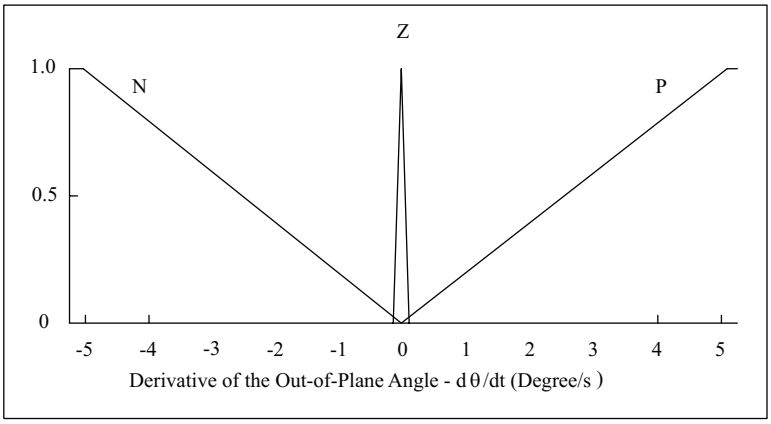

Figure 3.15: Fuzzification of $\dot{\theta}(t)$.

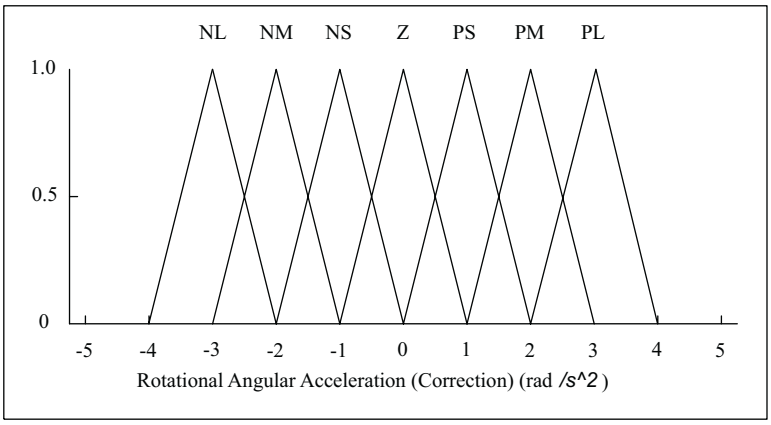

Figure 3.16: Defuzzification of $\ddot{\gamma}_{Correction}$.

Finally, after applying the rules, we defuzzify the output in order to find $\ddot{\gamma}_{Track}$. Figure 3.16 shows the fuzzy sets of $\ddot{\gamma}_{Correction}$.

Now, the output of this controller can be found according to

$$\ddot{\gamma}_{Reference}(t) = 0.6 \times \ddot{\gamma}_{Track} + 0.4 \times \ddot{\gamma}_{Correction} \tag{3.6}$$

3.3 Simulation Results

In order to test the performance of the designed controller, we used the MATLAB software [14] and its Fuzzy Logic Toolbox (V1.0) [13]. The toolbox provided a friendly Graphical User Interface (GUI), which made the testing faster and more efficient.

The first step in testing the controller was to generate an operator signal for testing. This signal was generated taking into consideration the actual crane model, which was built in the laboratory.

3.3.1 Radial Case (Gantry Case)

In this case, the cable length is set equal to 1.0 m, and the trolley is moved radially 0.75 m from $r = 0.25$ m to $r = 1.0$ m. The trolley accelerates for 3/8th of the cable period 0.75 s, moves at a constant velocity of 0.23078 m/s for 2.5 s, and decelerates for another 0.75 s, Figure 3.17. The whole operation is executed within 4.0 s. The acceleration amplitude is 0.3077 m/s^2. In Figure 3.18, we compare the controlled and uncontrolled in-plane oscillation angle associated with this movement. In the uncontrolled response, the oscillations continue with an amplitude of 6° without any damping. In fact, the uncontrolled payload oscillates with an amplitude of 3° after the acceleration period. When the deceleration occurs, it adds more energy to the payload oscillations, thereby raising the amplitude of oscillations to 6°. Closing the loop, we note that the initial kick of the in-plane angle is less than 2° during the acceleration phase and about $-2°$ during the deceleration phase. Also, we note that the oscillations are damped within about 5 s.

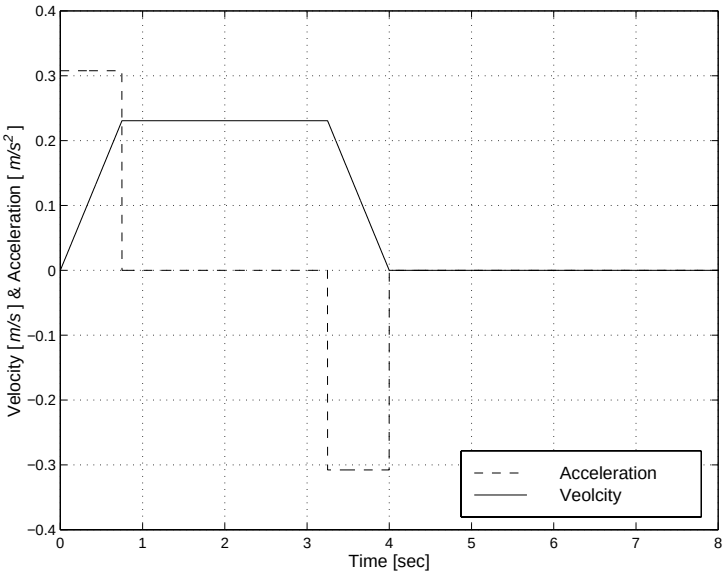

Figure 3.17: Operator radial signal.

The controller has no effect on the rotational angle $\gamma(t)$ or the out-of-plane oscillation

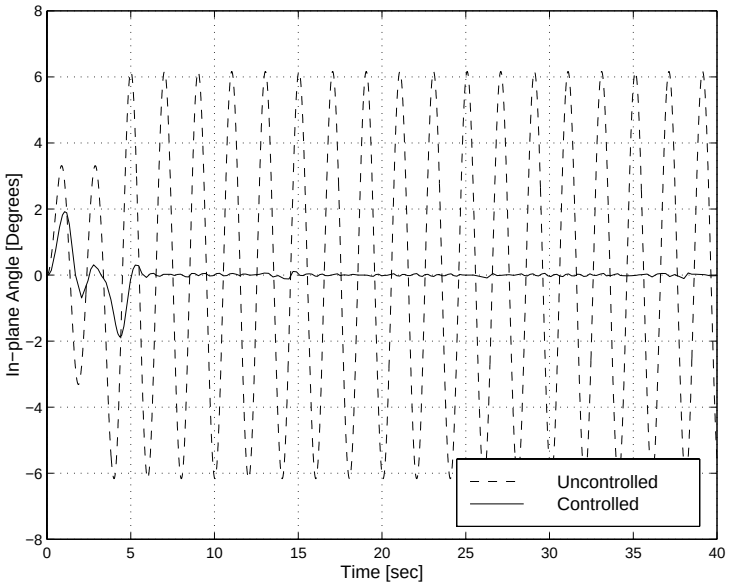

Figure 3.18: Uncontrolled vs controlled in-plane oscillation angle $\phi(t)$ for the gantry case using the fuzzy controller.

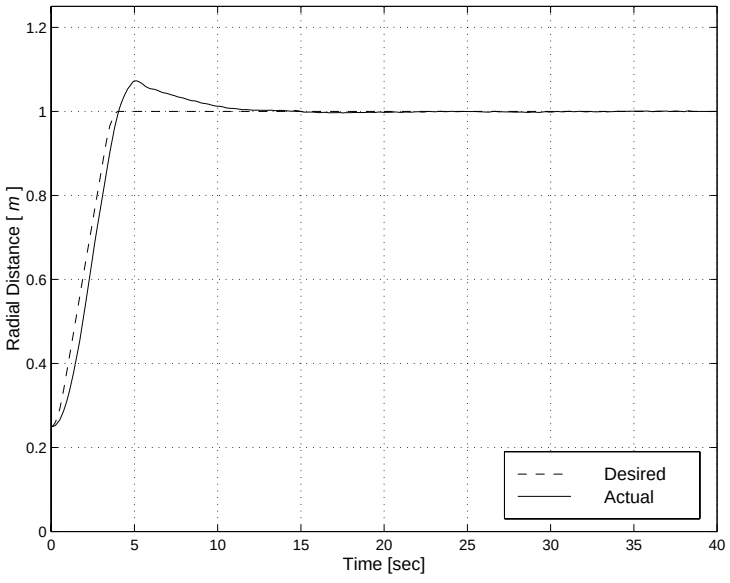

Figure 3.19: Desired and actual radial distances for the gantry case using the fuzzy controller.

angle $\theta(t)$. We also note that it takes about 15 s for the trolley to reach the end position, even though the oscillations are damped within 5 s. Figure 3.19 shows both the trolley desired position commanded by the operator and the actual position. The overshoot in the trolley position is somewhat large, about 7 cm. The trolley lags the operator command at the beginning, then catches up with an under-damped response. We note that the steady-state error is zero. So we conclude that the performance of the controller is good.

3.3.2 Rotational Case

For this case, the cable length is also set equal to 1.0 m, but the jib is rotated 90° from its initial position, and the trolley is set 1.0 m away from the center to magnify any oscillations due to the rotational motion. The jib rotates with an acceleration of 0.4928 rad/s^2 for 0.75 s, with a constant angular velocity of 0.3696 rad/s for 3.8 s, and then decelerates for another 0.75 s, Figure 3.20. Thus, the operation takes 5 s.

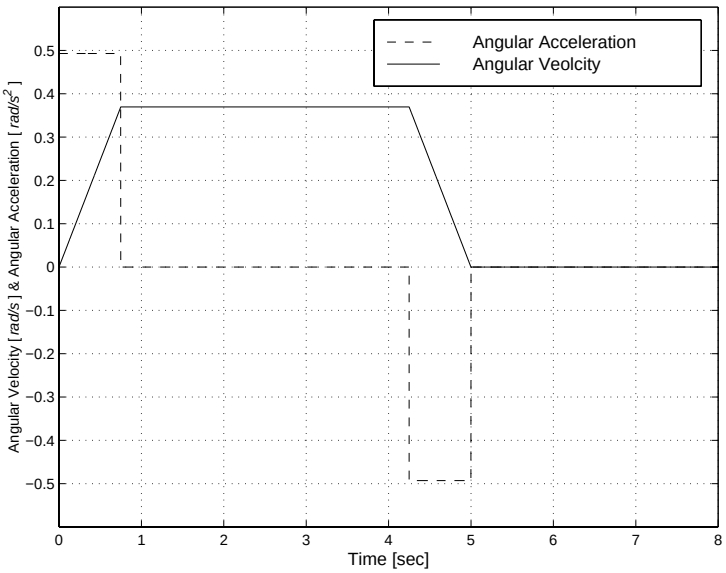

Figure 3.20: Operator rotational signal.

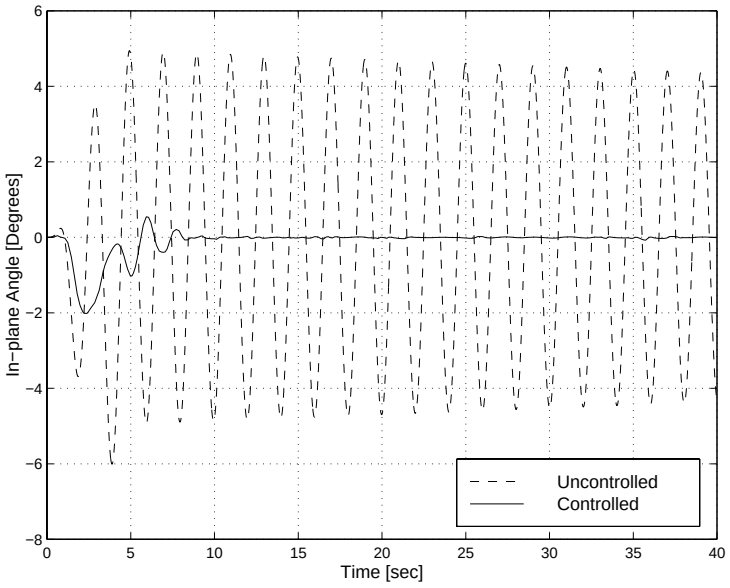

Figure 3.21: Uncontrolled vs controlled in-plane oscillation angle $\phi(t)$ for the rotational case using the fuzzy controller.

In Figures 3.21 and 3.22, we compare the controlled and the uncontrolled in-plane and out-of-plane angles. In the uncontrolled case, initially the in-plane angle increases slightly because the motion starts perpendicular to the jib plane, then the in-plane angle increases to more than 3.5° during the constant angular velocity phase due to the centrifugal force. Finally, the in-plane angle undergoes a persistent oscillation of more than 4°. On the other hand, the out-of-plane angle increases to more than 4.5° in the acceleration phase and persists afterwords. There is a continuous energy exchange between the in-plane and out-of-plane motions, resulting from a one-to-one internal resonance between these modes.

Closing the loop results in a decrease in both the in-plane and out-of-plane motions. The in-plane angel reaches -2° before it decays to almost zero in 10 s. On the other hand, the out-of-plane angle increases to approximately 4° before it decays to almost zero in 25 s. We see from Figures 3.22 to 3.23 that it takes about 20 s to reach the final state and to reduce the oscillation angles almost to zero, which is a long time for such a small model.

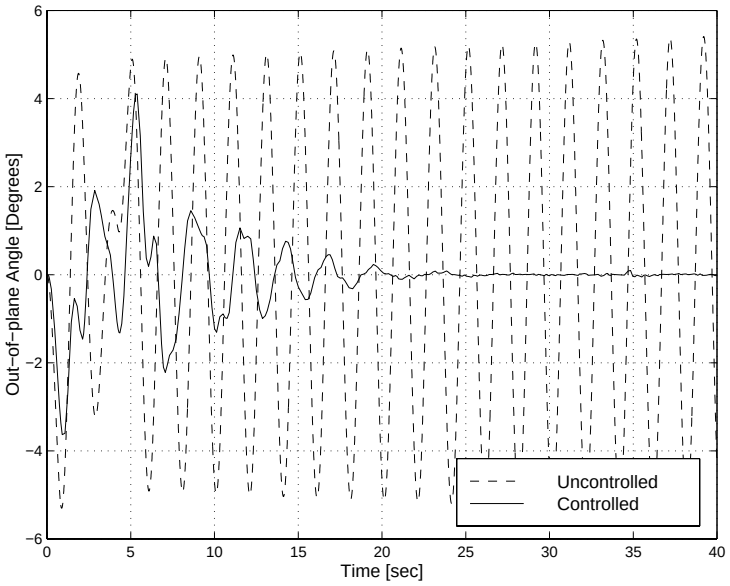

Figure 3.22: Uncontrolled vs controlled out-of-plane oscillation angle $\theta(t)$ for the rotational case using the fuzzy controller.

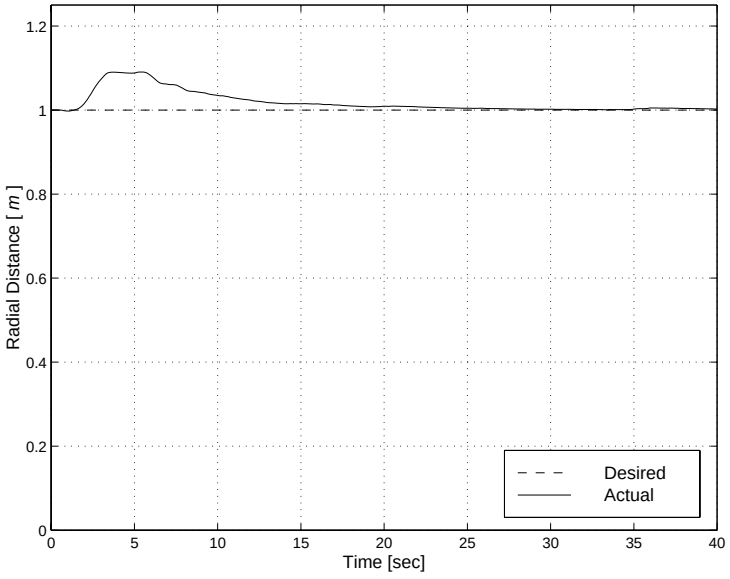

Figure 3.23: Desired and actual radial distances for the rotational case using the fuzzy controller.

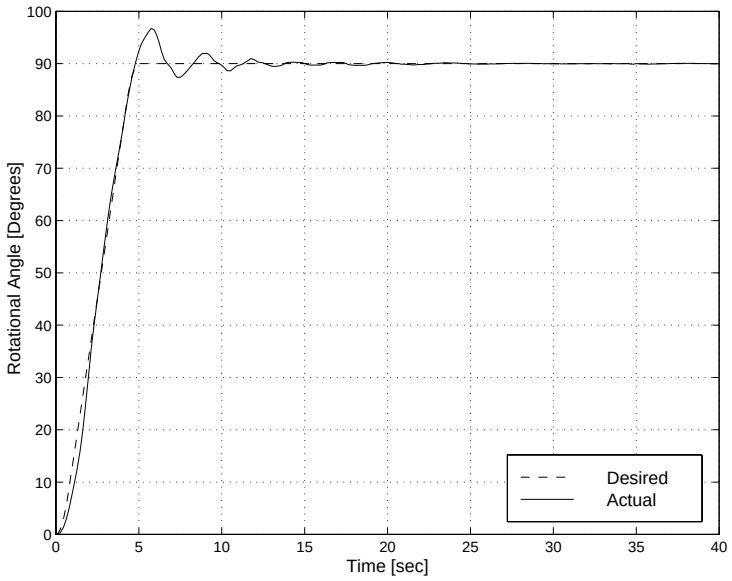

Figure 3.24: Desired and actual rotational angles for the rotational case using the fuzzy controller.

In order to damp the oscillations in the in-plane angle, the trolley needs to be moved about 10 cm from its initial position, which is considered to be a large deviation. As for the rotational angle of the jib, it has experienced a moderate overshoot of about 7°, Figure 3.24. So even though the controller showed good performance in keeping the oscillation angles small, the time of the maneuver is somewhat large.

3.3.3 Compound Case

In this case, a combination of the radial and rotational motions is applied. The trolley is moved on the jib a distance of 0.75 m as in the radial case, while the jib is rotated 90° around the tower as in the rotational case. We compare in Figures 3.25 and 3.26 the controlled and uncontrolled in-plane and out-of-plane angles. Again, in the uncontrolled case, energy is being continuously exchanged between the two modes of oscillations due to the one-to-one internal resonance between them. The in-plane angle grows to more than 7° in 40 s, whereas

the out-of-plane angle reaches more than 9° in 5 s. Figures 3.25 and 3.26 show that the oscillation period of the payload is 2 s.

Closing the loop results in a significant reduction in both angles. The in-plane angle grows to about 2.5° in the deceleration period, but it then decreases to almost zero within 10 s. On the other hand, the out-of-plane angle increases initially to almost 5° before it decays to almost zero in 25 s. This settling time is considered long for such a small model.

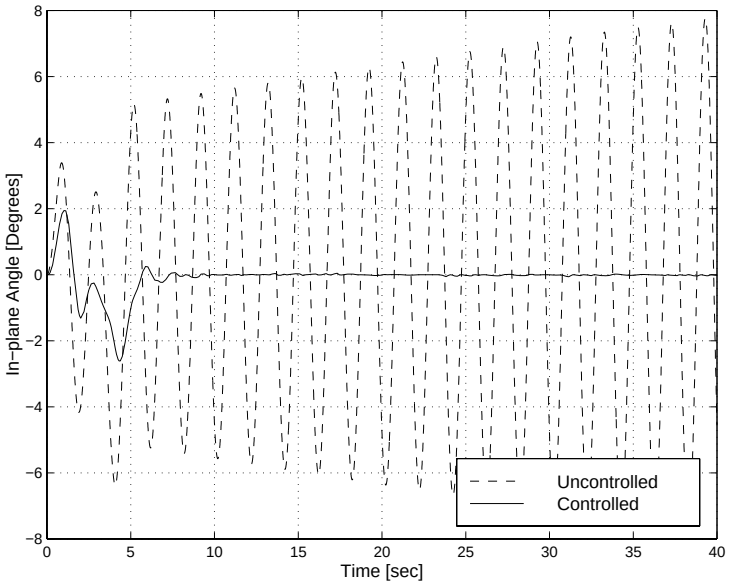

Figure 3.25: Uncontrolled vs controlled in-plane oscillation angle $\phi(t)$ for the compound case using the fuzzy controller.

Figure 3.27 shows the radial distance of the trolley on the jib. A problem that is clear here is that the overshoot is large, about 20 cm. With this large overshoot, the trolley takes more than 15 s to reach its end position, which is a long time for such a small model. As for the rotational angle of the jib, its overshoot is reasonable, about 8°. But Figure 3.28 shows that it also takes a long time to settle like the trolley, about 12 s.

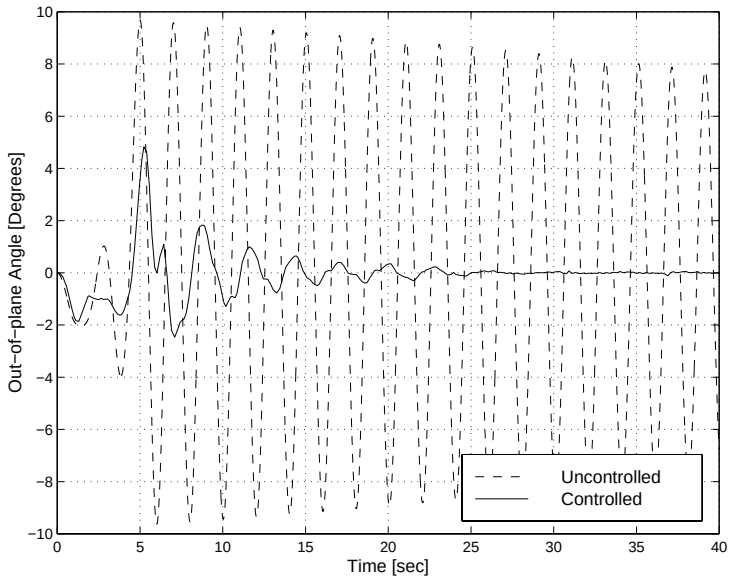

Figure 3.26: Uncontrolled vs controlled out-of-plane oscillation angle $\theta(t)$ for the compound case using the fuzzy controller.

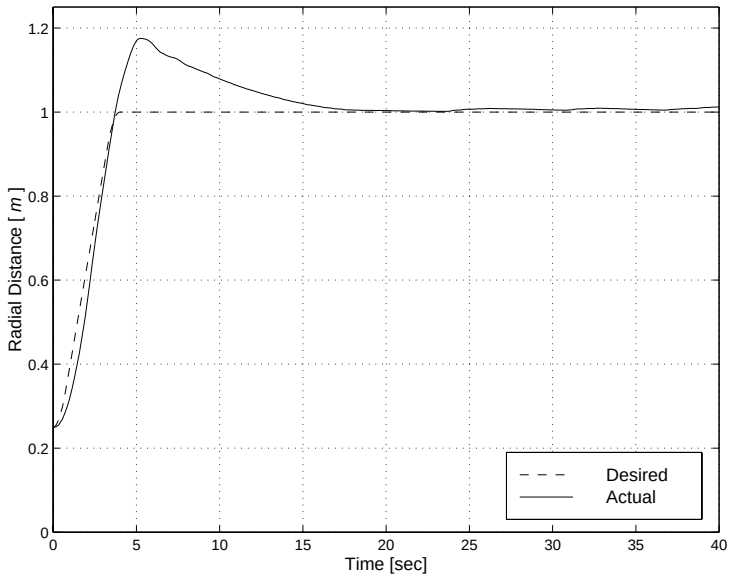

Figure 3.27: Desired and actual radial distances for the compound case using the fuzzy controller.

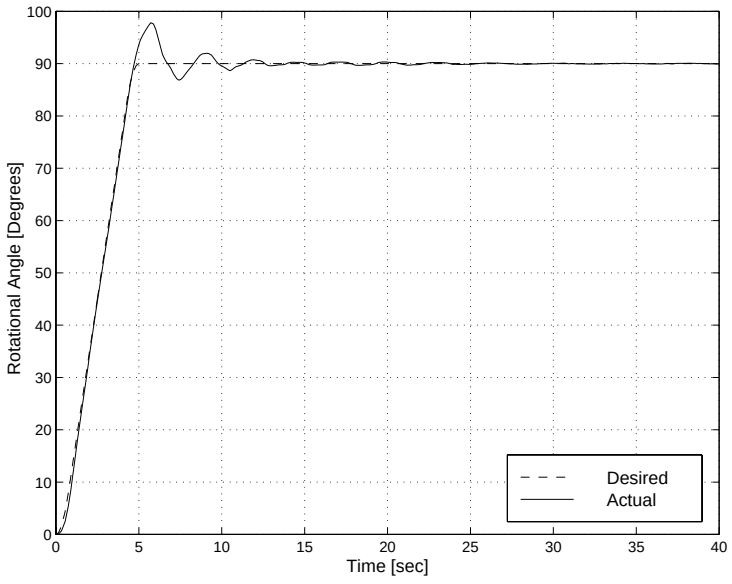

Figure 3.28: Desired and actual rotational angles for the compound case using the fuzzy controller.

3.3.4 Damping Case

In this case, we investigate the effectiveness of the controller to damp initial disturbances. We started with an initial disturbance of 75° for each of the oscillation angles $\theta(t)$ and $\phi(t)$. The trolley is placed at a distance of 1.0 m on the jib to magnify the oscillations effect. In Figures 3.29 and 3.30, we compare the controlled and uncontrolled in-plane and out-of-plane motions. Because the model does not include damping, the uncontrolled angles continue to oscillate with an amplitude of 75° forever. On the other hand, applying the controller, we find that the in-plane motion decays below 10° after 8 s and to almost zero within 20 s. In contrast, the damping of the out-of-plane motion is much slower. It takes about 18 s for this motion to decay below 10° and it takes about 25 s for it to decay to almost zero.

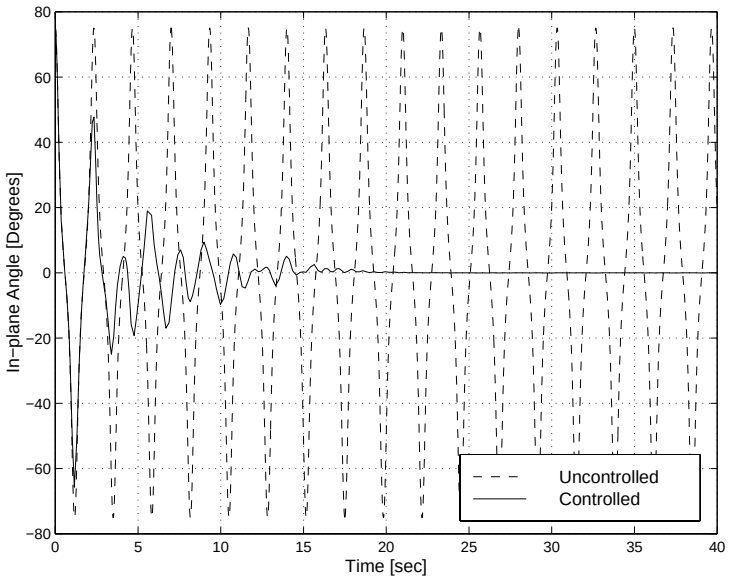

Figure 3.29: Uncontrolled vs controlled in-plane oscillation angle $\phi(t)$ for the damping case using the fuzzy controller.

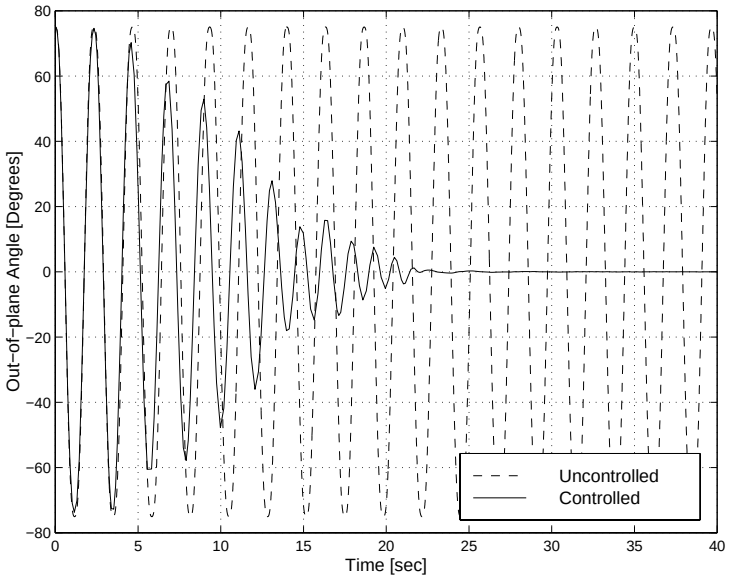

Figure 3.30: Uncontrolled vs controlled out-of-plane oscillation angle $\theta(t)$ for the damping case using the fuzzy controller.

In Figures 3.31 and 3.32, we show the deviations of the trolley position and the rotational angle of the jib from their desired values. The maximum deviation of the trolley from the desired distance (1.0 m) is about 10 cm, which is small. Moreover, the maximum swing of the rotational angle of the jib to damp the oscillations is less than 10°, which is also considered to be small. Even though the time taken to damp these large initial disturbances is somewhat long, the trolley and jib deviations needed to damp these oscillations are considered to be small. This gives the fuzzy logic controller an advantage in cases where the trolley or the jib can not be moved as fast and the damping time is not important.

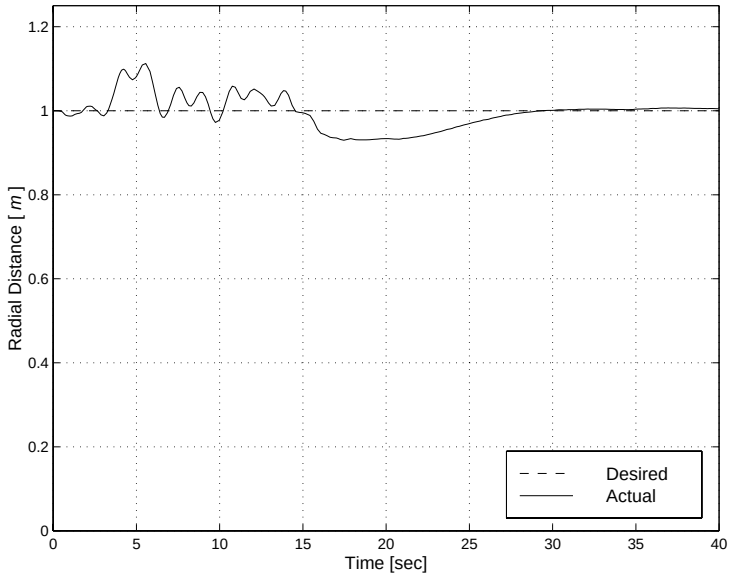

Figure 3.31: Desired and actual radial distances for the damping case using the fuzzy controller.

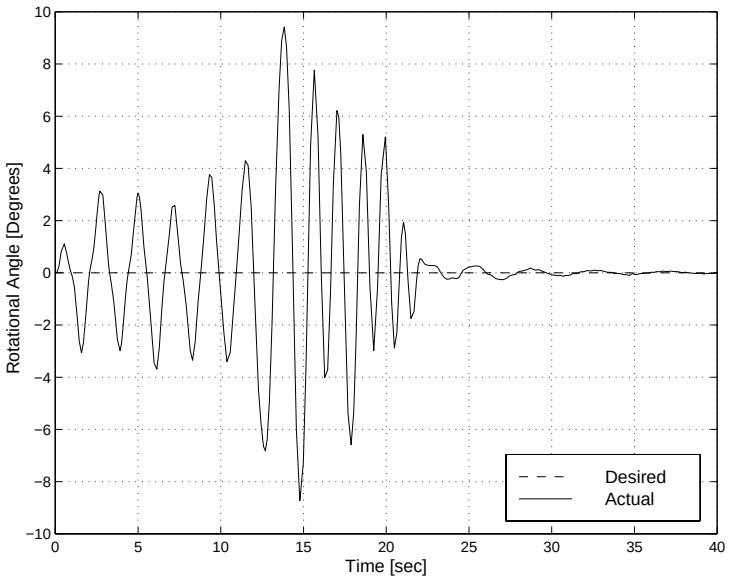

Figure 3.32: Desired and actual rotational angles for the damping case using the fuzzy controller.

Chapter 4

Delay Feedback Controller

The delayed-position controller for cranes was first introduced by Masoud et al. [6]. It was applied to ship-mounted boom cranes and showed excellent results both in simulations and in experiments. The time-delayed position feedback controller, which we will refer to as the delay controller, is a nonlinear controller. By design, the controller should work for any type of crane because of its independence of the crane structure and dynamics apart from the hoisting cable length.

4.1 Introduction

The delay controller does not modify the operator input, instead it adds a correction to the operator signal to account for the load oscillations. This results in a desired crane motion that produces the least oscillations. The delay-feedback controller, Figure 4.1, uses the oscillation angels of the hoisting cable and the current radial position of the trolley as input signals to generate the correction signal. Summations of the controller outputs constitute reference signals for both the radial and angular motions of the crane. Since the inputs to the system dynamics are angular and radial accelerations, tracking blocks have to be added

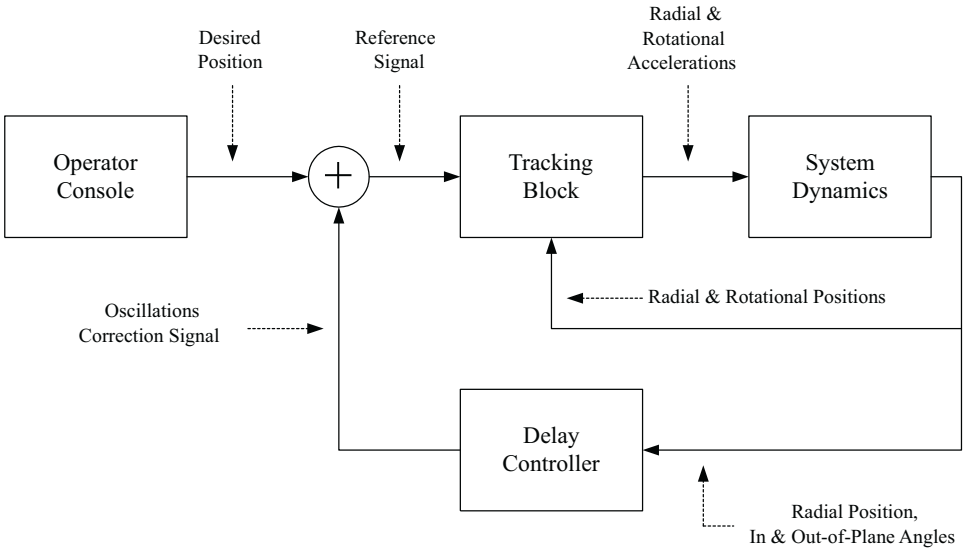

Figure 4.1: System block diagram with delay controller.

to make sure that the desired accelerations are fed to the system. The tracking blocks have the positions, whether angular or radial, as feedback signals.

4.2 One-Dimensional Model

We start with the one-dimensional model [5], as shown in Figure 4.2. The delay controller is based on feeding back a time-delayed percentage of the position of the load with respect to the suspension point. The correction signal generated by the controller is given by

$$r_c = kl \sin\left(\phi(t-\tau)\right) \tag{4.1}$$

where τ is a time delay, k is the controller gain, and r_c is the radial position correction. Adding this correction to the operator radial input r_o results in the reference radial signal

$$r_{ref} = r_o + kl \sin\left(\phi(t-\tau)\right) \tag{4.2}$$

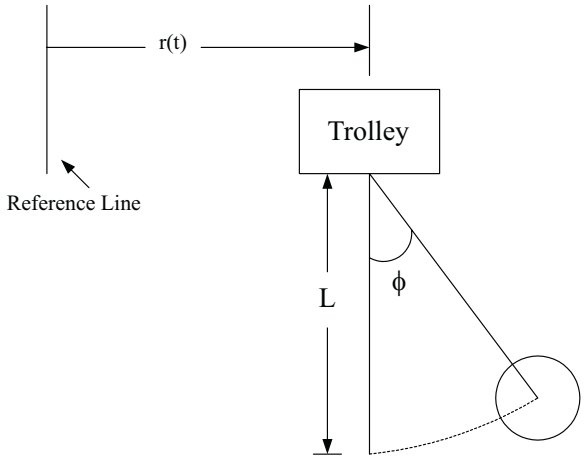

Figure 4.2: One-dimensional delay controller.

Equation 4.2 is then substituted into the equations of motion (2.18) and (2.19) to obtain the equations of motion of the controlled system.

A stability analysis of this system was performed by Henry et al. [7]. The result is shown in Figure 4.3 where the unshaded region corresponds to stable operations and the shaded areas correspond to unstable operations. Even in the stable region, the performance of the system varies according to the damping created by varying k and τ. Figure 4.4 shows contours of constant damping within the stable region, the darker the shade is, the higher the damping is. For example, if the period of the pendulum is 1 second, then the highest damping will occur at $k = 0.4$ and $\tau = 0.27sec$.

4.3 Two-Dimensional Model

For rotary cranes, the one-dimensional model is not sufficient so a two-dimensional model is developed. Because we can split the motion into two orthogonal planes, a similar control approach and a stability analysis are still valid. The gains and delays can be chosen to be

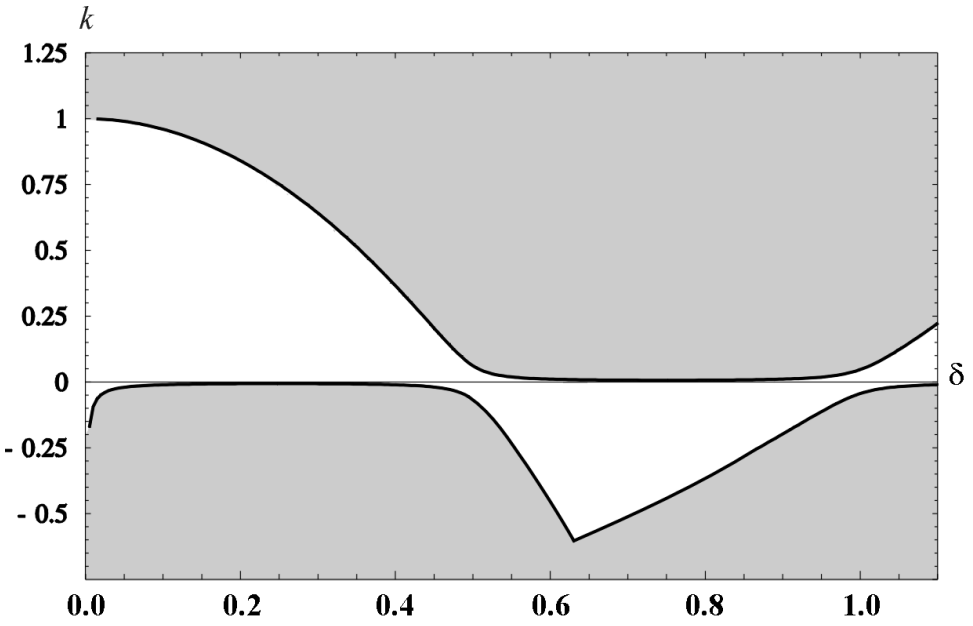

Figure 4.3: Stability of the delay controller.

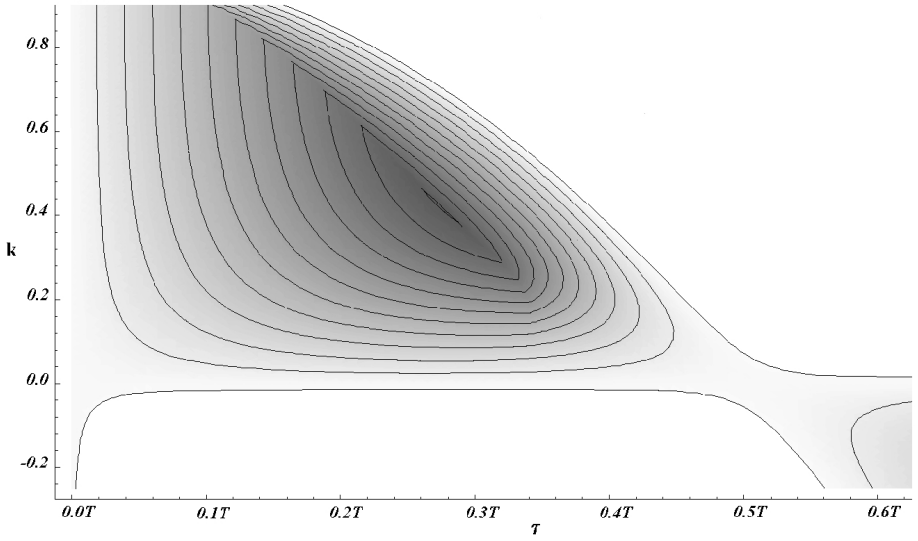

Figure 4.4: Damping as a function of the gain k and delay τ, where T is the pendulation period.

different for each axis. In cases where oscillations in one plane are expected to be higher than in the other, this can be very useful. Figure 4.5 shows a top view of a rotary crane, the jib lies along the x-axis. The load is hanging from point A on the trolley, the trolley is now at a distance r from the center. In order to dampen the motion, the trolley has to be moved from its current position A to point B over the time-delayed projection of the load cable. From the previous definitions of the in-plane angle $\phi(t)$ and out-of-plane angle $\theta(t)$, we find that

$$x_c(t) = -k_1 l \sin\left(\phi(t-\tau_1)\right)\cos\left(\theta(t-\tau_1)\right) \tag{4.3}$$

$$y_c(t) = k_2 l \sin\left(\theta(t-\tau_2)\right) \tag{4.4}$$

From geometry, we can deduce that

$$\delta_\gamma = \arctan\left(-\frac{y_c(t)}{r(t)+x_c(t)}\right) \tag{4.5}$$

and

$$\delta_r = \sqrt{y_c^2(t)+(r(t)+x_c(t))^2} - r(t) \tag{4.6}$$

It is clear now that we can calculate the previous corrections using the delayed angles, and by adding these corrections to the current operator input, we can calculate the reference signal.

4.4 Tracking Block

The inputs to the system dynamics block are radial and angular acceleration, while the signals generated by the delay controller are position signals. Thus, another controller is needed to input the correct accelerations to the system, which will make the trolley and jib take the same positions as those desired by the delay controller.

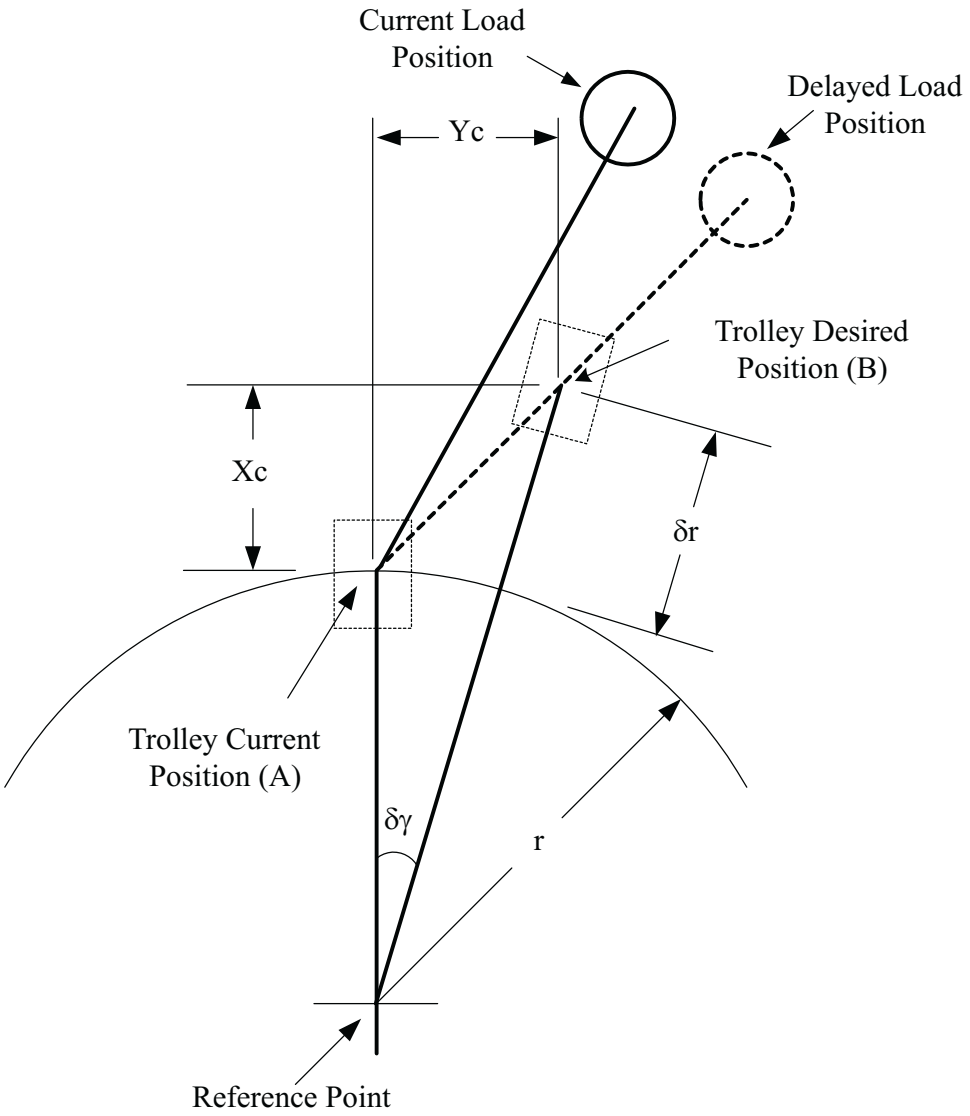

Figure 4.5: Top view of a rotary crane.

We redefine a new set of state-space equations in terms of the system states (x_1 to x_8) and the desired states (x_{1d} to x_{8d}) as follows:

$$y_1 = x_1 = \theta(t) \tag{4.7}$$

$$y_2 = x_2 = \phi(t) \tag{4.8}$$

$$y_3 = x_3 = r(t) \tag{4.9}$$

$$y_4 = x_4 = \gamma(t) \tag{4.10}$$

$$y_5 = x_3 - x_{3d} = r(t) - r_d(t) \tag{4.11}$$

$$y_6 = x_6 = \dot{r}(t) \tag{4.12}$$

$$y_7 = x_4 - x_{4d} = \gamma(t) - \gamma_d(t) \tag{4.13}$$

$$y_8 = x_8 = \dot{\gamma}(t) \tag{4.14}$$

$$u_1 = \ddot{r}(t) \tag{4.15}$$

$$u_2 = \ddot{\gamma}(t) \tag{4.16}$$

Substituting equations (4.11) and (4.13) into equations (4.15) and (4.16) yields

$$u_1 = \ddot{x}_{3d} + \ddot{y}_5 \tag{4.17}$$

$$u_2 = \ddot{x}_{4d} + \ddot{y}_7 \tag{4.18}$$

Then $\ddot{y}_5$ and $\ddot{y}_7$ are calculated as follows:

$$\ddot{y}_5 = -2\lambda\dot{y}_5 - \lambda^2 y_5 \tag{4.19}$$

$$\ddot{y}_7 = -2\lambda\dot{y}_7 - \lambda^2 y_7 \tag{4.20}$$

By taking the Laplace transform of equations (4.19) and (4.20), we have

$$s^2 Y_5(s) + 2\lambda s Y_5(s) + \lambda^2 Y_5(s) = 0 \tag{4.21}$$

$$s^2 Y_7(s) + 2\lambda s Y_7(s) + \lambda^2 Y_7(s) = 0 \tag{4.22}$$

For stable solutions of equations (4.21) and (4.22), λ has to be positive. Hence, the tracking block outputs are given by

$$u_1 = \ddot{x}_{3d} - 2\lambda\dot{y}_5 - \lambda^2 y_5 \tag{4.23}$$

$$u_2 = \ddot{x}_{4d} - 2\lambda\dot{y}_7 - \lambda^2 y_7 \tag{4.24}$$

For a fast response, λ is chosen to be large ($\lambda = 100$).

4.5 Simulation Results

A procedure similar to that used to test the fuzzy logic controller is used to test the delay controller. For the ease of comparison, the same operator signal is used. Through out the simulations, the delay time and gain used are $\tau = 0.56$ seconds and $k = 0.4$.

4.5.1 Radial Case (Gantry Case)

Similar to the test of the fuzzy logic controller, the cable length is set equal to 1.0 m, and the trolley is moved from $r = 0.25$ m to $r = 1.0$ m. The trolley accelerates for 3/8th of the cable period 0.75 s, moves at a constant velocity for 2.5 s, and decelerates for another 0.75 s, Figure 3.17. The whole operation is executed within 4.0 s. The acceleration amplitude is

$0.3077 m/s^2$. In Figure 4.6, we compare the in-plane oscillation angle associated with this movement obtained with the fuzzy logic and delay controllers.

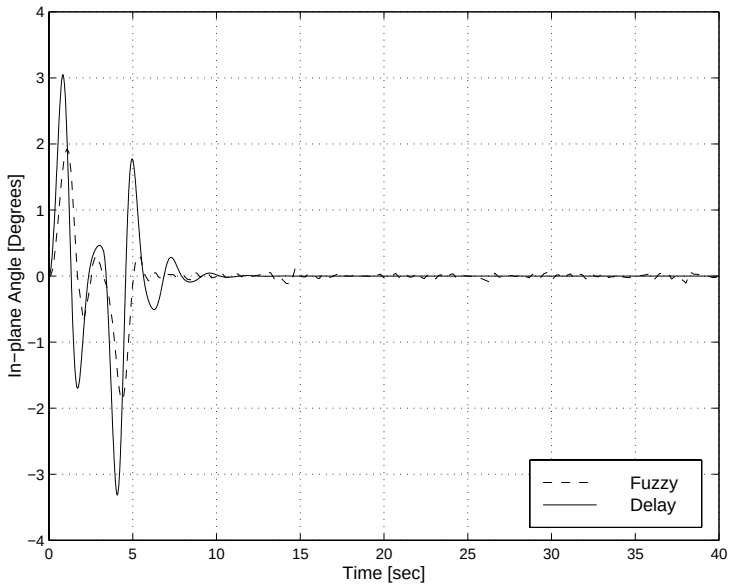

Figure 4.6: Controlled in-plane oscillation angle $\phi(t)$ for the gantry case using the delay and fuzzy controllers.

With the delay controller, the in-plane angle resulting from the trolley acceleration is about 3°, which is larger than that obtained with the fuzzy controller, about 2°. During the deceleration phase, the in-plane angle reaches less than -3° in the case of the delay controller compared with about -2° in the case of the fuzzy controller. Also, we note that the oscillations are damped within about 10 s using the delay controller, which is also longer than the 5 s taken by the fuzzy controller.

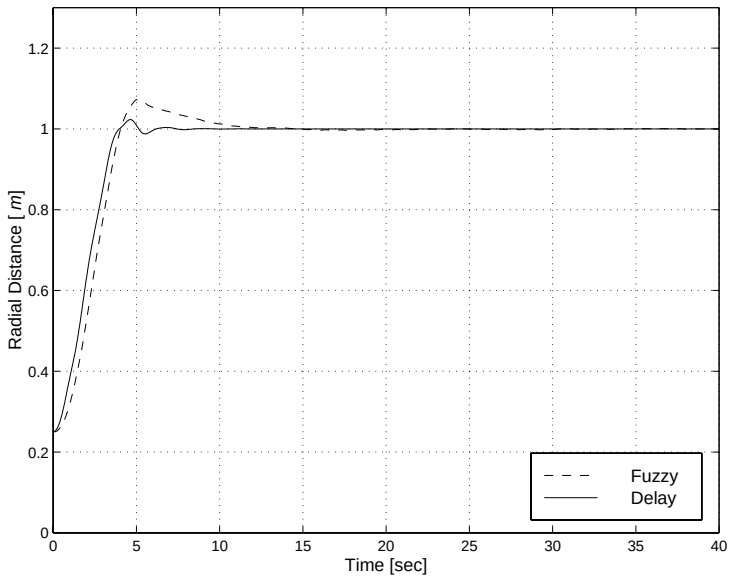

Figure 4.7: Radial distance for the gantry case using the delay and fuzzy controllers.

In Figure 4.7, we compare the actual trolley motion using the delay and fuzzy controllers. The trolley does not lag the operator command as in the case of the fuzzy controller. The trolley motion is under-damped in both cases. While it takes the trolley about 7 s to settle in its end position using the delay controller, it takes 12 s using the fuzzy controller. The overshoot in the trolley position obtained with the delay controller is about 3 cm, which is small compared to 7 cm obtained with the fuzzy controller. We note that the steady-state error is zero in both cases. None of the controllers has any effect on the rotational angle $\gamma(t)$ or the out-of-plane oscillation angle $\theta(t)$. We note that the delay controller is faster than the fuzzy controller in the sense that the trolley reaches the end position in a shorter time compared with that needed by the fuzzy controller. However, the in-plane angle amplitude obtained with the fuzzy controller is less than that achieved by the delay controller, which can be more important than the settling time in some applications.

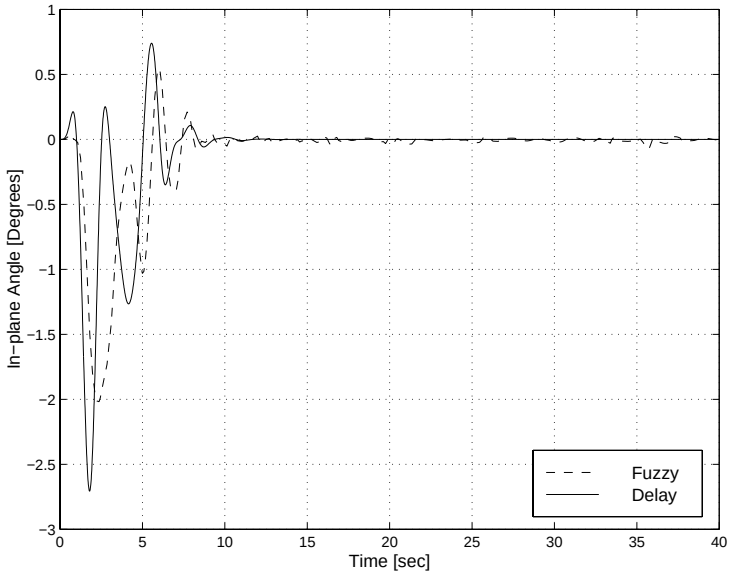

Figure 4.8: Controlled in-plane oscillation angle $\phi(t)$ for the rotational case using the delay and fuzzy controllers.

4.5.2 Rotational Case

For this case, the cable length is also set equal to 1.0 m, but the jib is rotated 90° from its initial position, and the trolley is set at a radius of 1.0 m to magnify any oscillations due to the rotational motion. The jib rotates with an acceleration of 0.4928 rad/s^2 for 0.75 s, with a constant angular velocity for 3.5 s, and then decelerates for another 0.75 s, Figure 3.20. Thus, the operation takes 5 s.

In Figures 4.8 and 4.9, we compare the in-plane and out-of-plane angles obtained with the fuzzy logic and delay controllers. When the delay controller is used, the in-plane angle increases slightly during the acceleration phase, then decreases to less than $-2.5°$ during the constant angular velocity phase, and decreases to about 1° during the deceleration phase. Finally, the in-plane motion decays to almost zero in less than 10 s of the start of the operation. We note that the fuzzy controller takes the same time as the delay controller to damp the in-plane angle, but its maximum is about 2°.

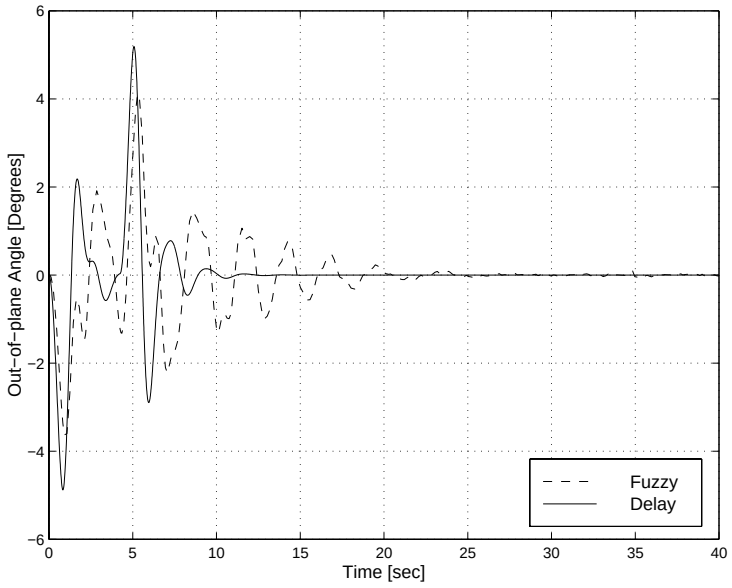

Figure 4.9: Controlled out-of-plane oscillation angle $\theta(t)$ for the rotational case using the delay and fuzzy controllers.

When looking at the effect of the delay controller on the out-of-plane angle, we see that it starts increasing during the acceleration phase because the jib motion is tangential to the out-of-plane motion. It follows from Figure 4.9 that the buildup of the out-of-plane angle is negative because the load lags behind the jib while it accelerates. The second large motion buildup occur when the jib stops and the load continue to travel. Even though the out-of-plane angle increases more than the in-plane angle in the initial phase, the controller is able to damp both of them in 10 s, which is very small compared to the 25 s needed by the fuzzy controller to damp the out-of-plane angle. Still the fuzzy controller has the advantage of having lower oscillation amplitudes.

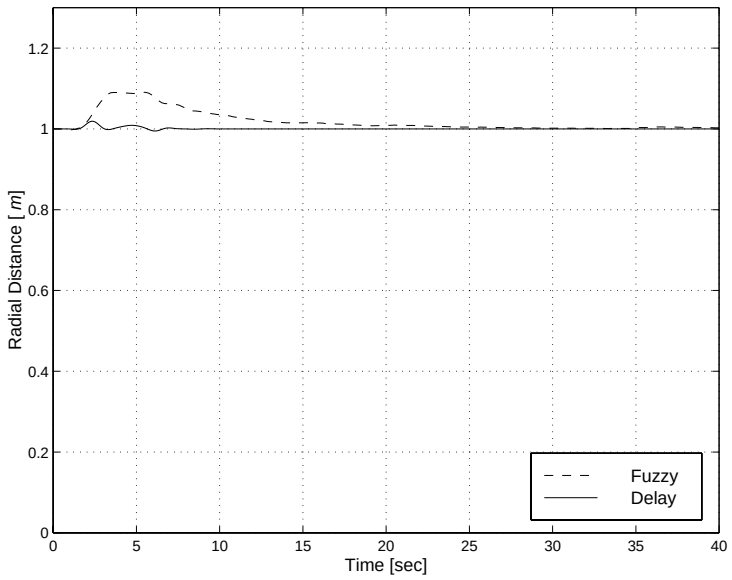

Figure 4.10: Radial distance for the rotational case using the delay and fuzzy controllers.

Figure 4.10 shows that, to damp the in-plane and out-of-plane oscillations using the delay controller, the trolley need to move about 2 *cm* from its initial position, which is about 1/4th the motion needed by the fuzzy controller. In addition, we note that it takes a longer time for the trolley to reach its end position using the fuzzy controller. On the other hand, it follows from Figure 4.11 that the rotational angle of the jib experiences an overshoot of about 3°, compared to 7° in the case of the fuzzy controller. It follows from Figures 4.10 to 4.11 that it takes about 10 *s* for the trolley and the jib to reach the end position and at the same time reduce the oscillation angles to almost zero, which is almost half the time needed by the fuzzy logic controller.

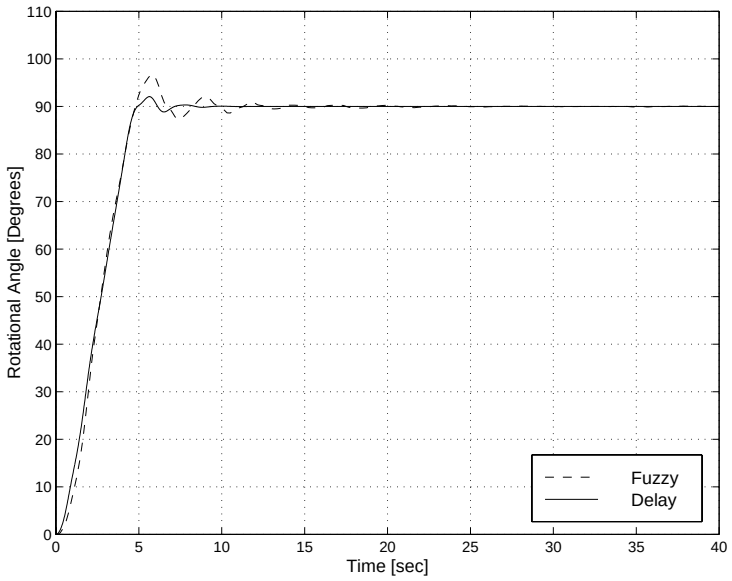

Figure 4.11: Rotational angle for the rotational case using the delay and fuzzy controllers.

4.5.3 Compound Case

In this case, a combination of the radial and rotational motions is applied. The trolley is moved on the jib a distance of 0.75 m as in the radial case, while the jib is rotated 90° around the tower as in the rotational case. In Figures 4.12 and 4.13, we compare the delay and fuzzy logic controlled in-plane and out-of-plane angles, respectively. When the delay controller is used, the in-plane angle reaches a maximum of about 4° during the deceleration phase, which is larger than the 2.5° obtained with the fuzzy controller. It follows from Figure 4.12 that the in-plane oscillations are damped within 10 s using either controller. Initially, the in-plane angle has a positive kick due to the radial acceleration and then a moderate negative kick due to the centrifugal force. When the trolley decelerates, it kicks the load away, resulting in a larger negative kick. When the delay controller is used the out-of-plane angle $\theta(t)$ reaches a maximum value of approximately 6°, and it takes about 10° to damp, as in the case of the in-plane angle, Figures 4.13. But with the fuzzy controller, it takes more

time (about 25 s) to damp the 5° out-of-plane angle.

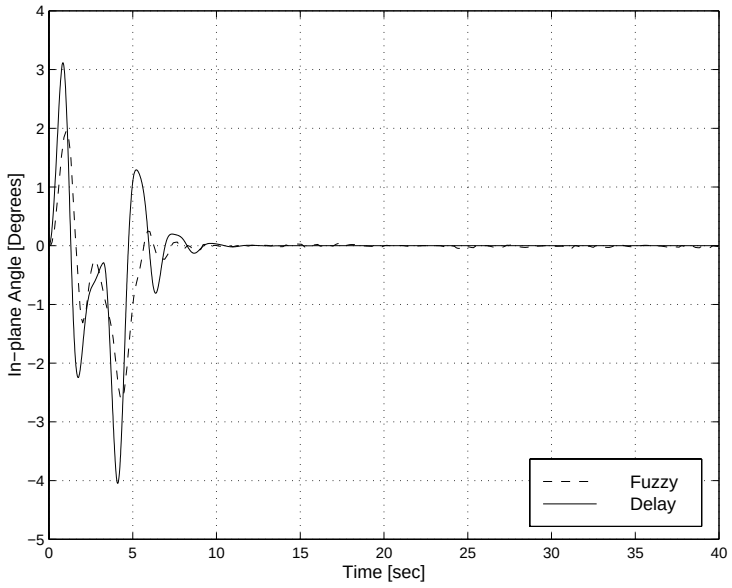

Figure 4.12: Controlled in-plane oscillation angle $\phi(t)$ for the compound case using the delay and fuzzy controllers.

Figure 4.14 shows the radial distance of the trolley on the jib. Using the delay controller, the overshoot is small (about 2 cm), which is 1/10th that needed by the fuzzy case. With this small overshoot, the trolley takes less than 8 s to reach its end position, which is a short time for this model and far less than the 17 s needed by the fuzzy controller. As for the jib rotational angle, Figure 4.15 shows that the overshoot (about 3°) needed by the delay controller is smaller than the 7° needed by the fuzzy controller.

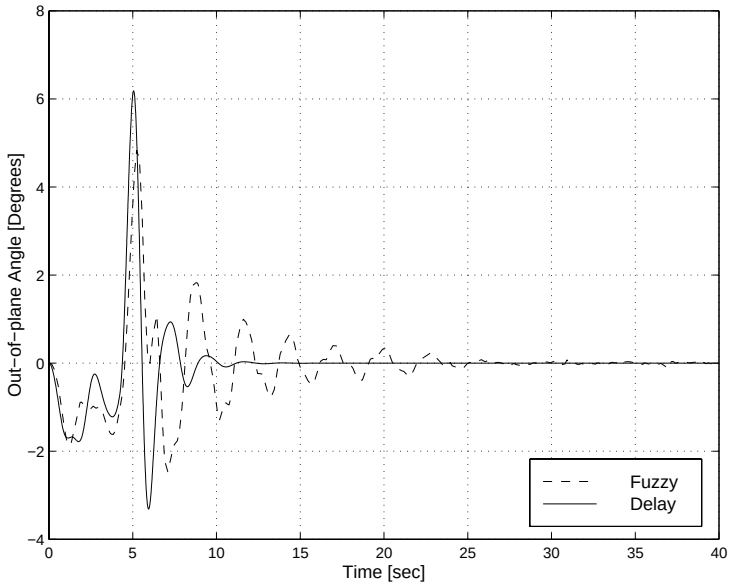

Figure 4.13: Controlled out-of-plane oscillation angle $\theta(t)$ for the compound case using the delay and fuzzy controllers.

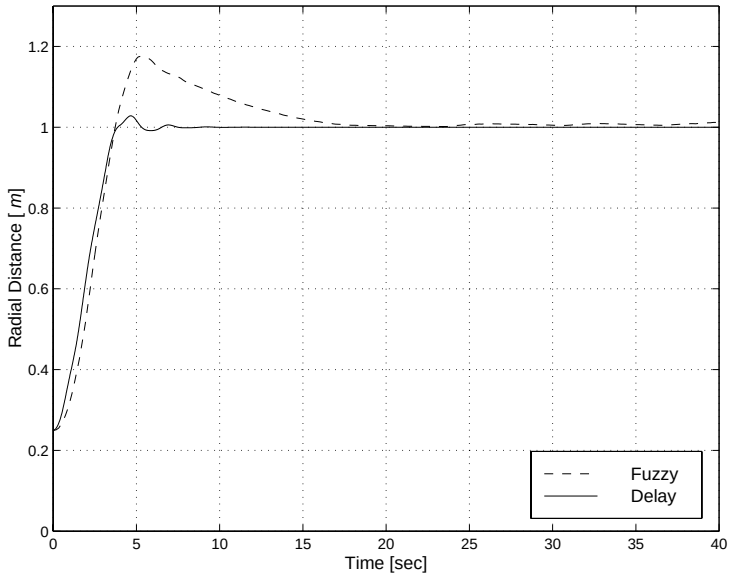

Figure 4.14: Radial distance for the compound case using the delay and fuzzy controllers.

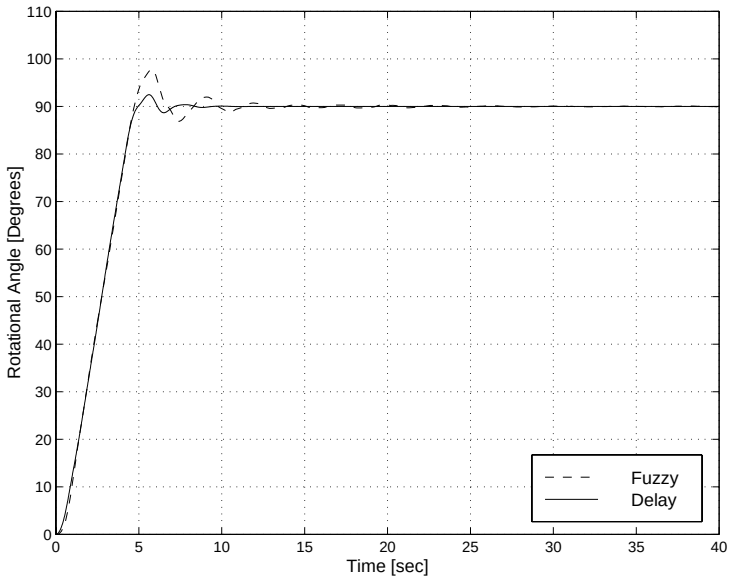

Figure 4.15: Rotational angles for the compound case using the delay and fuzzy controllers.

4.5.4 Damping Case

In this case, we investigate the effectiveness of the controller to damp initial disturbances. We start with an initial condition of 75° for each of the oscillation angles $\theta(t)$ and $\phi(t)$. The trolley is placed at a distance of 1.0 m on the jib to magnify the oscillations effect. In Figures 4.16 and 4.17, we compare the fuzzy and delay controlled in-plane and out-of-plane motions, respectively. The delay controller is more effective in damping this initial disturbance than the fuzzy controller. The in-plane and out-of-plane angles damp in less than 8 s, which is very small compared to the 25 s needed by the fuzzy controller. We note that the rate of damping for the out-of-plane angle with the fuzzy controller is very slow.

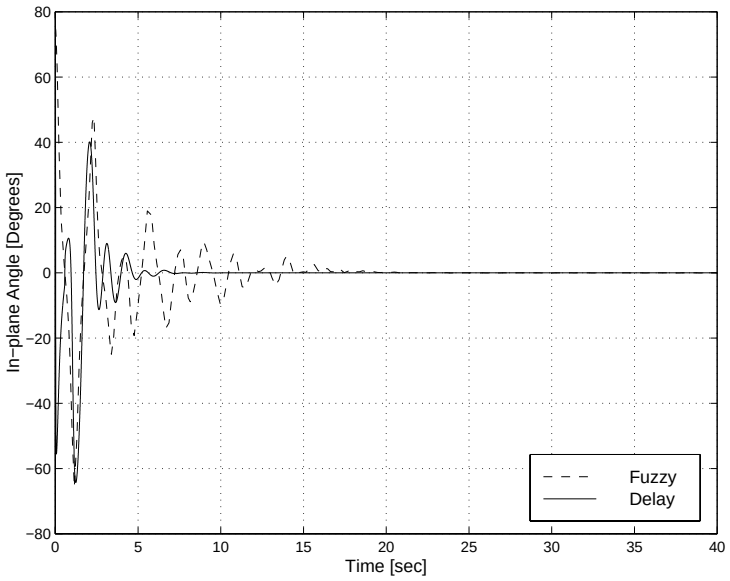

Figure 4.16: Controlled in-plane oscillation angle $\phi(t)$ for the damping case using the delay and fuzzy controllers.

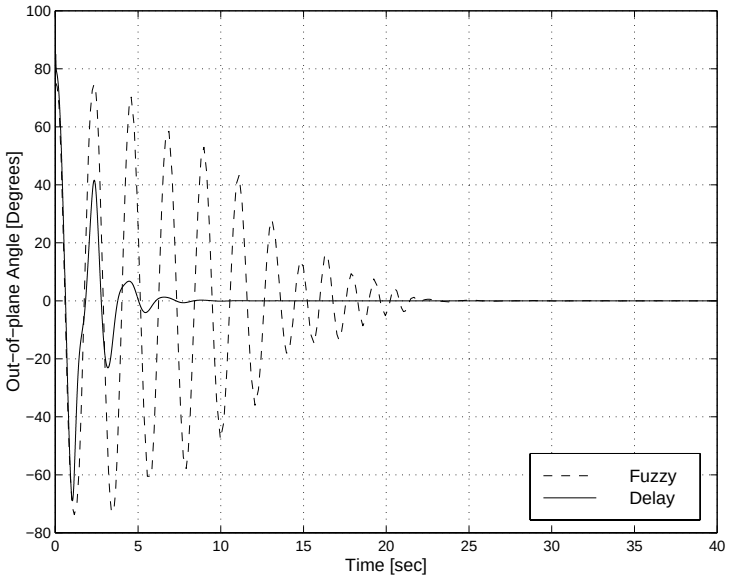

Figure 4.17: Controlled out-of-plane oscillation angle $\theta(t)$ for the damping case using the delay and fuzzy controllers.

It follows from Figures 4.18 and 4.19 that the control action represented by the radial and rotational deviations from the rest position are large in the case of the delay controller. The trolley's maximum deviation from the 1.0 m distance is about 30 cm, which is three times that needed by the fuzzy controller. Also the maximum swing of the jib's rotational angle needed to damp the oscillations is about 23°, which is also larger than the 10° needed by the fuzzy controller. On the other hand, we note that the time taken to damp these large initial disturbance is very small, due to the large trolley and jib deviations. This gives the fuzzy logic controller an advantage in cases where the trolley or the jib can not be moved as fast and large and the damping time is not of great importance. However, in cases where the damping time is more important, the delay controller is more advantageous for damping the oscillations.

Finally, one important thing to note is that the fast deviations of the trolley and jib from their rest positions might not be realizable in practice because of limitations on the motor's acceleration, which consequently will lead to slowing down the damping of the disturbance.

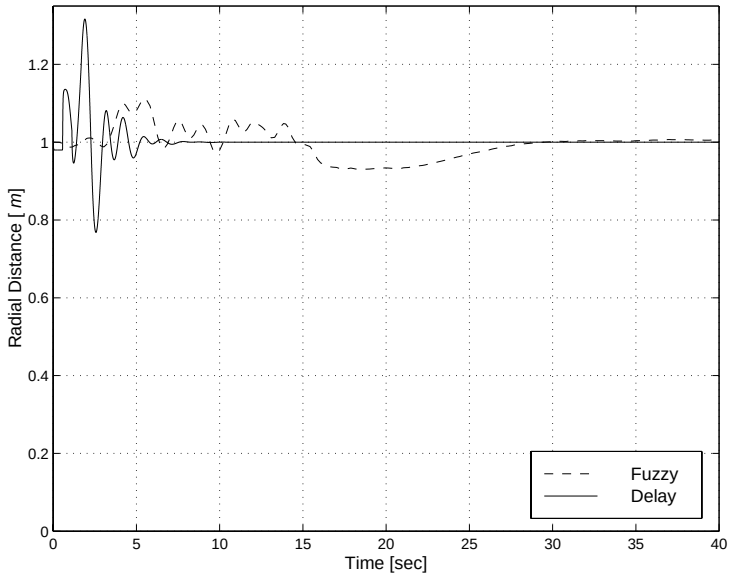

Figure 4.18: Radial distance for the damping case using the delay and fuzzy controllers.

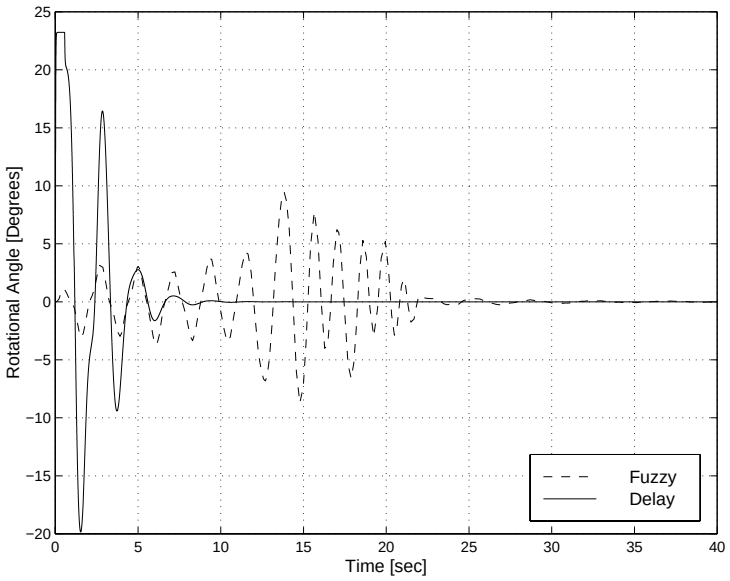

Figure 4.19: Rotational angles for the damping case using the delay and fuzzy controllers.

Effect of the gain variation on the performance of the delay controller

In the absence of large initial disturbances is able to damp the oscillations in a short time and with a low overshoot. But when large initial disturbances are present, the trolley and jib motions needed to damp these initial disturbances become large. With the flexibility built in the delay controller to vary the damping rate, one can choose to lower the gain k from 0.4 to 0.16, while keeping the delay period $\tau = 0.56\ s$. This reduction in the gain reduces the damping rate but increases the settling time. The advantage of reducing the gain is a reduction in the maximum trolley and jib deviations needed to damp the initial disturbances.

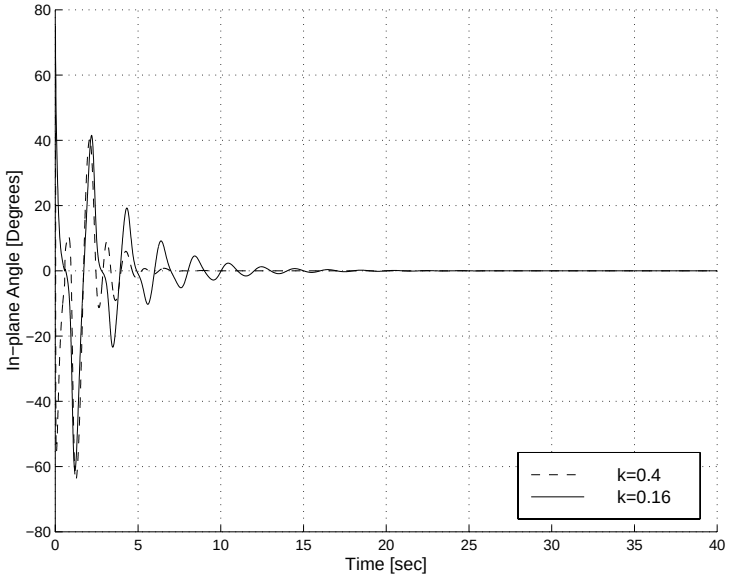

Figure 4.20: Controlled in-plane oscillation angle $\phi(t)$ for the damping case using the delay controller with different gains.

Figures 4.20 and 4.21 show the delay controlled in-plane and out-of-plane angles with different values for the gain k. We note that the settling time for the in-plane angle has increased from 6 s to 15 s. Similarly, the out-of-plane settling time has increased from 7 s to 20 s.

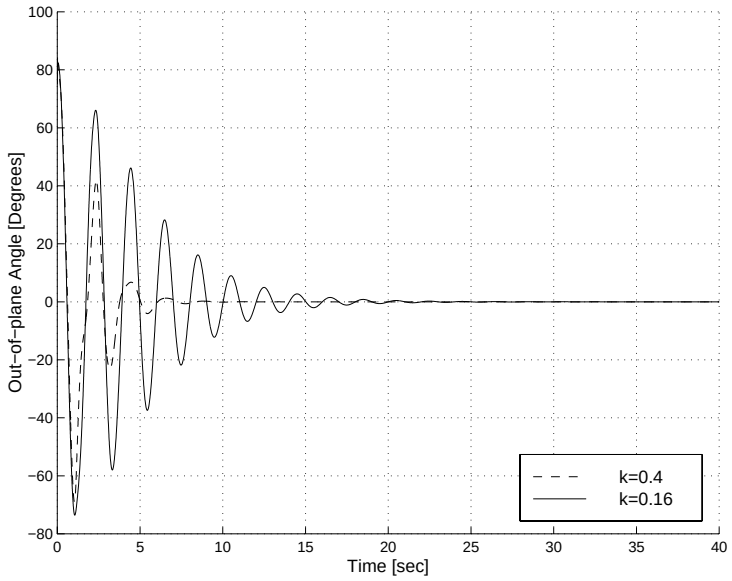

Figure 4.21: Controlled out-of-plane oscillation angle $\theta(t)$ for the damping case using the delay controller with different gains.

Figures 4.22 and 4.23 show the deviations of the trolley and jib from their rest positions. The trolley deviation from the 1.0 m position is decreased from more than 30 cm to 8 cm when the gain is reduced from 0.4 to 0.16. Moreover, the jib deviation is decreased from 23° to 9° with the reduction of the gain. This shows the flexibility of tuning the delay controller according to the needs of the operation environment.

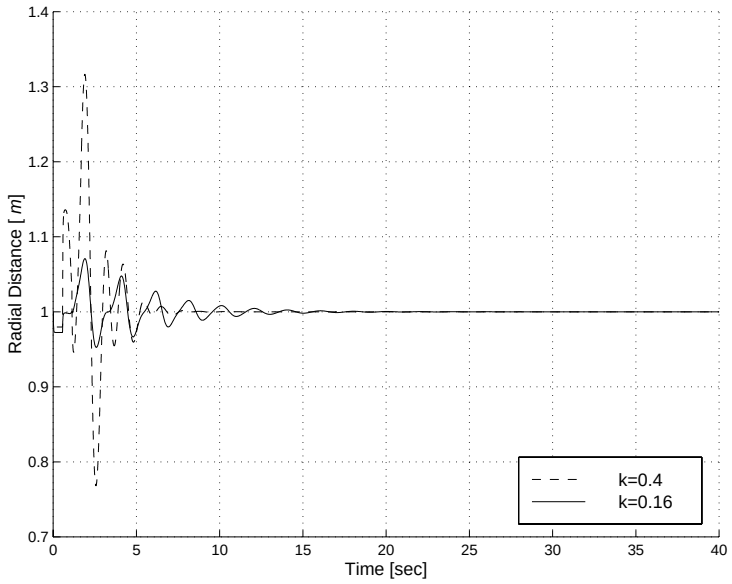

Figure 4.22: Radial distances for the damping case using the delay controller with different gains.

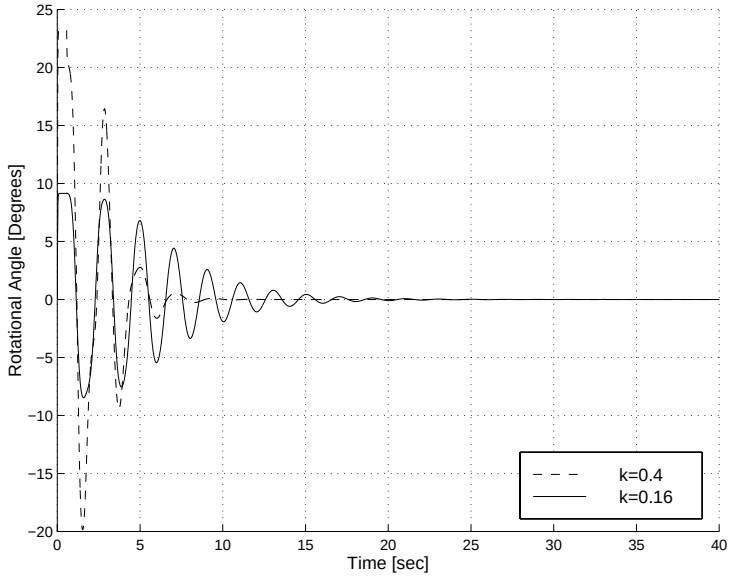

Figure 4.23: Rotational angles for the damping case using the delay controller.

When comparing the results of the delay controller with the reduced gain $k = 0.16$ with those of the fuzzy controller, we note that the delay controller damps the oscillations in a short time, less than 20 s, compared to the 25 s needed by the fuzzy controller to achieve the same task. This is provided that the delay controller is able to achieve the initial kick in the trolley and jib positions.

4.6 Hybrid Controller

A combination of the delay and fuzzy controllers is investigated, as show in Figure 4.24. The fuzzy logic tracking engines are used to control the positions of the trolley and the jib to make sure that they are close to the operator input. The same tracking FIEs used in the fuzzy controller are used here, with the same rules and ranges except that the radial FIE output is scaled with a factor of 1/5. Since the output of the fuzzy engines is either acceleration or angular acceleration, double integrators are used to generate the position signals. On the other hand, the delay controller is used to generate the correction signal that is responsible for reducing the load oscillations, exactly as done in the delay controller. The combination of the modified desired position signal and the oscillations correction signal is passed to the tracking block, which generates the acceleration input to the system dynamics block.

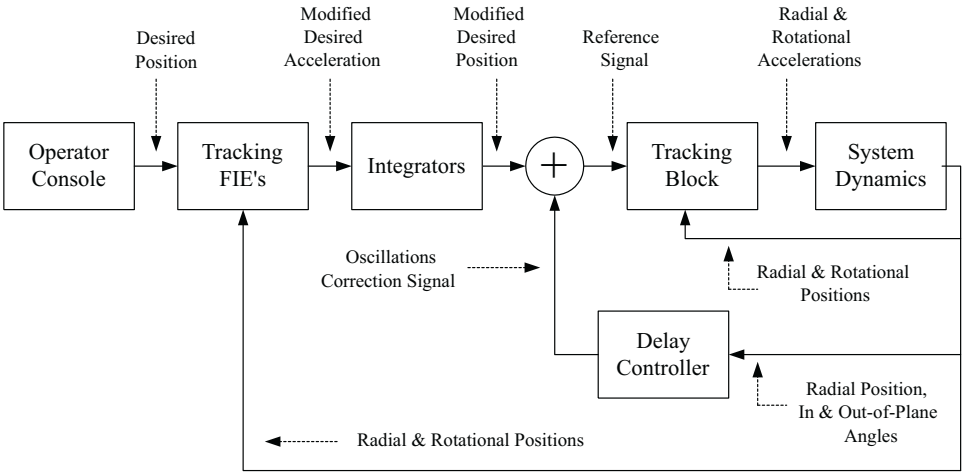

Figure 4.24: System block diagram of the hybrid controller.

To investigate the performance of the hybrid controller, we perform simulations for the cases considered earlier in investigating the performances of the fuzzy and delay controllers.

4.6.1 Radial Case (Gantry Case)

Similar to what we did with the previous two controllers, the cable length is set equal to 1.0 m and the trolley is moved 0.75 m from $r = 0.25$ m to $r = 1.0$ m. The trolley accelerates for 3/8th of the cable period 0.75 s, moves at a constant velocity for 2.5 s, and decelerates for another 0.75 s, Figure 3.17. The whole operation is executed within 4.0 s. The acceleration amplitude is 0.3077 m/s^2. In Figure 4.25, we compare the fuzzy, delay, and hybrid controlled in-plane oscillation angle associated with this movement. For the hybrid controller, we note an initial kick of about 1.5° in the in-plane angle during the acceleration phase. A kick of a similar amplitude but in the negative direction occurs during the deceleration phase. However, during the constant velocity phase the oscillations are very small. The maximum in-plane kick in this case is smaller than those 2° and 3° obtained, respectively, with both the fuzzy and delay controllers. Also we note that the oscillations damp within about 10 s,

which is again larger than the 5 s obtained with the fuzzy controller, but comparable to that of the delay controller.

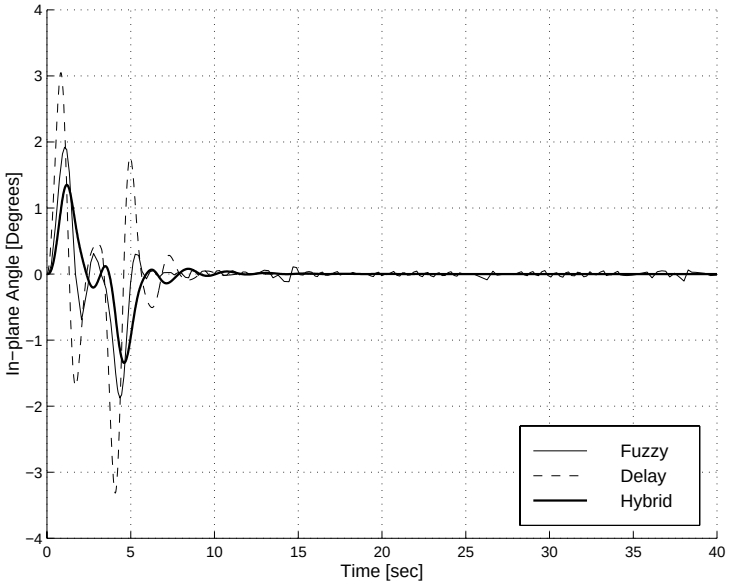

Figure 4.25: Controlled in-plane oscillation angle $\phi(t)$ for the gantry case using the delay, fuzzy, and hybrid controllers.

This controller has no effect on either the rotational angle $\gamma(t)$ or the out-of-plane oscillation angle $\theta(t)$. Figure 4.26 shows the actual trolley position for all of the three controllers. We note that with the hybrid controller, the trolley lags the operator command at the beginning of the motion even more than the fuzzy controller. The trolley has an under-damped response, with the steady-state error being zero. The overshoot in this case is about 10 cm, which is larger than the 7 cm needed by the fuzzy controller to damp the oscillations. We note also that it takes about 20 s for the trolley to reach the end position, which is the largest needed time among the three controllers. Overall, the performance of the controller is good, especially if the application under consideration has strict oscillation requirements. But if the oscillation requirements are relaxed, then the delay controller is faster than both the fuzzy and hybrid controllers.

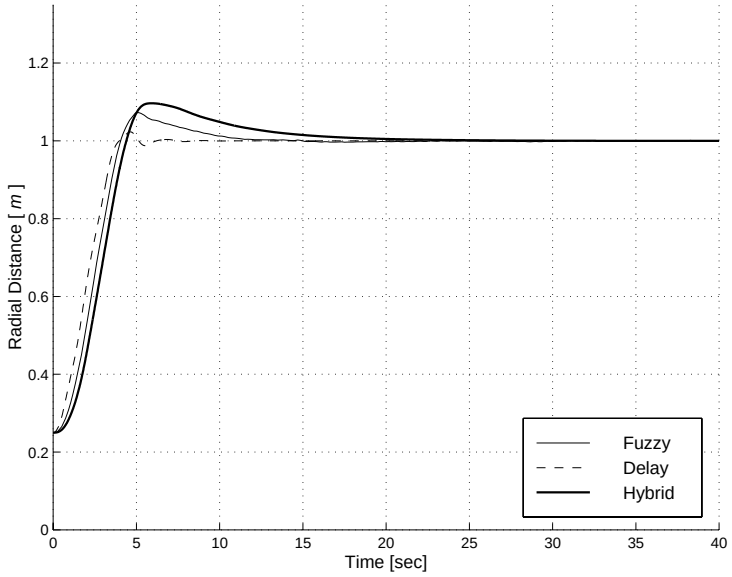

Figure 4.26: Radial distance for the gantry case using the delay, fuzzy, and hybrid controllers.

4.6.2 Rotational Case

The cable length is also set equal to 1.0 m, but the jib is rotated 90° from its initial position, and the trolley is set 1.0 m away from the center to magnify any oscillations due to the rotational motion. The jib rotates with an acceleration of 0.4928 rad/s^2 for 0.75 s, with a constant angular velocity for 3.5 s, and a deceleration of 0.4928 rad/s^2 for another 0.75 s, Figure 3.20. Thus, the operation takes 5 s.

Again not only the out-of-plane angle $\theta(t)$ experiences a disturbance in the rotational case, Figure 4.27, but also the amplitude of oscillation of the in-plane angle $\phi(t)$ reaches about 3.5° with the hybrid controller, Figure 4.28. This amplitude is larger than those obtained with both the fuzzy logic and delay controllers, 2° and 2.75°, respectively. This large amplitude occurs during the constant velocity phase and is attributed to the centrifugal force. It follows from Figure 4.28 that the hybrid controller takes about 20 s to reduce the in-plane oscillations to zero, which is a long time when compared to the times needed by the fuzzy and delay

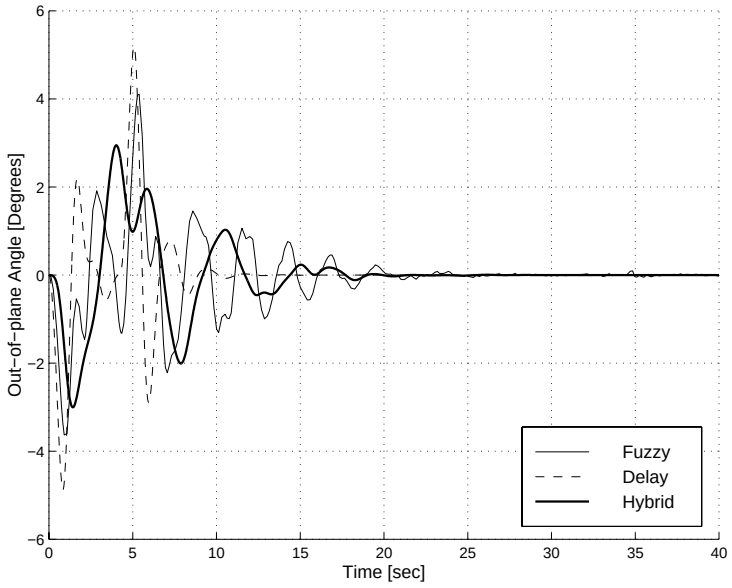

Figure 4.27: Controlled out-of-plane oscillation angle $\theta(t)$ for the rotational case using the delay, fuzzy, and hybrid controllers.

controllers. It follows from Figure 4.27 that the hybrid controlled out-of-plane angle starts initially with a negative amplitude of -3° during the acceleration phase and then experiences a positive amplitude of 3° during the deceleration phase, where the jib stops and the load continues to pendulate. The maximum initial out-of-plane angle is smaller than that of the in-plane angle. It is also smaller than that obtained using the fuzzy and delay controllers.

It follows from Figure 4.29 that, in order to damp the oscillation angles with the hybrid controller, the trolley needs to move about 2 cm from its initial position, which is comparable to the motion needed by the delay controller. On the other hand, it follows from Figure 4.30 that the jib rotational angle experiences an overshoot of about 15°, which is very large compared to the 3° needed by the delay controller or even the 7° needed by the fuzzy controller. Overall, it takes about 20 s for the system to reach its final state and reduce the oscillation angles to zero, which is almost twice the time required by the delay controller.

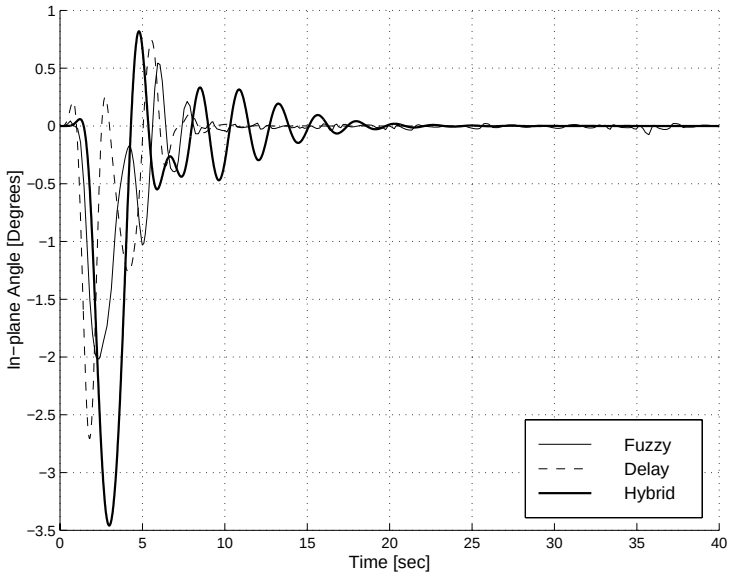

Figure 4.28: Controlled in-plane oscillation angle $\phi(t)$ for the rotational case using the delay, fuzzy, and hybrid controllers.

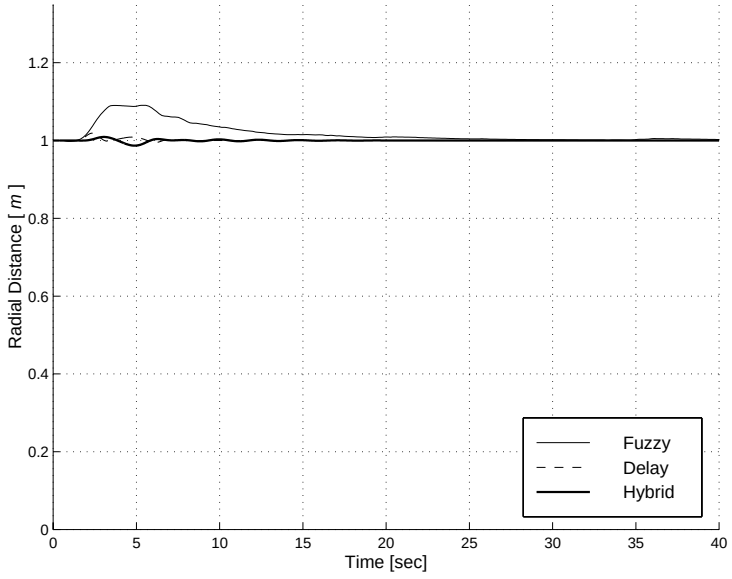

Figure 4.29: Radial distances for the rotational case using the delay, fuzzy, and hybrid controllers.

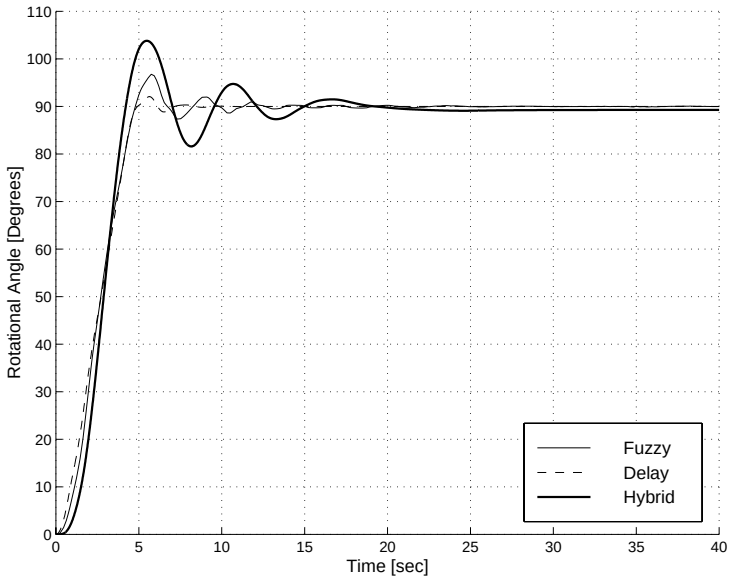

Figure 4.30: Rotational angles for the rotational case using the delay, fuzzy, and hybrid controllers.

4.6.3 Compound Case

In this case, a combination of the radial and rotational motions is applied. The trolley is moved on the jib a distance of 0.75 m as in the radial case, while the jib is rotated 90° around the tower as in the rotational case. In Figures 4.31 and 4.32, we compare the fuzzy, delay, and hybrid controlled in-plane and out-of-plane angles, respectively. The hybrid controller is very effective in reducing the uncontrolled response. With the hybrid controller, the in-plane angle increases to about 1.25° due to the radial acceleration. Then, it increases to 2.5° during the deceleration phase, which is slightly larger than that obtained with the fuzzy controller, but smaller than the 4° obtained with the delay controller. However, the in-plane oscillations are damped within about 18 s, which is longer than the 10 s needed by either the delay or fuzzy controller. It follows from 4.32 that, with the hybrid controller, the out-of-plane angle $\theta(t)$ reaches a maximum amplitude of approximately 3°, and it takes almost 18 s to damp

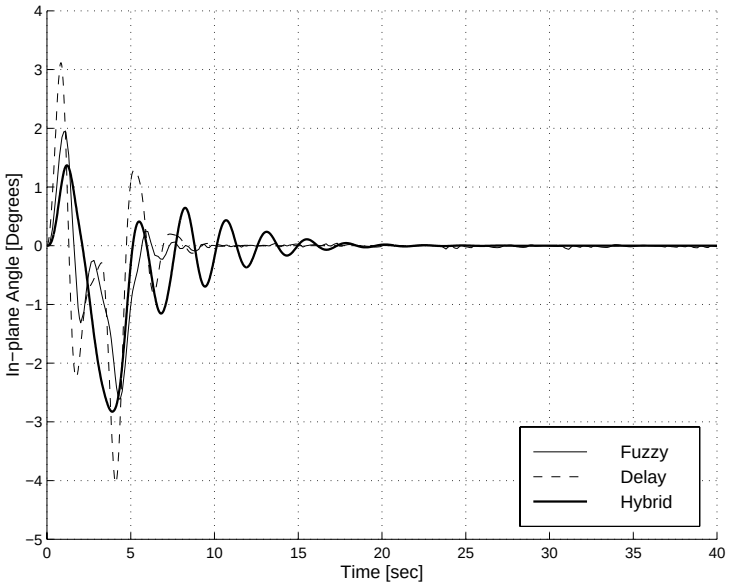

Figure 4.31: Controlled in-plane oscillation angle $\phi(t)$ for the compound case using the delay, fuzzy, and hybrid controllers.

as in the case of the in-plane angle. This response is much better than that obtained with the delay and fuzzy controllers. We note that, in this case, the maximum amplitude of oscillation is 3°, compared with the 5° and 6° obtained with the fuzzy and delay controllers, respectively.

Figure 4.33 shows the radial distance of the trolley on the jib. As in the case of the fuzzy controller, the overshoot needed by the hybrid controller is large, about 10 cm. With this large overshoot, the trolley takes about 17 s to reach its end position, which is a long time for such a model. It follows from Figure 4.34 that the overshoot of the rotational angle is also large, about 15°, which is larger than the 7° overshoot obtained with the fuzzy controller and the 3° overshoot obtained with the delay controller. This is besides the long settling time of 20 s.

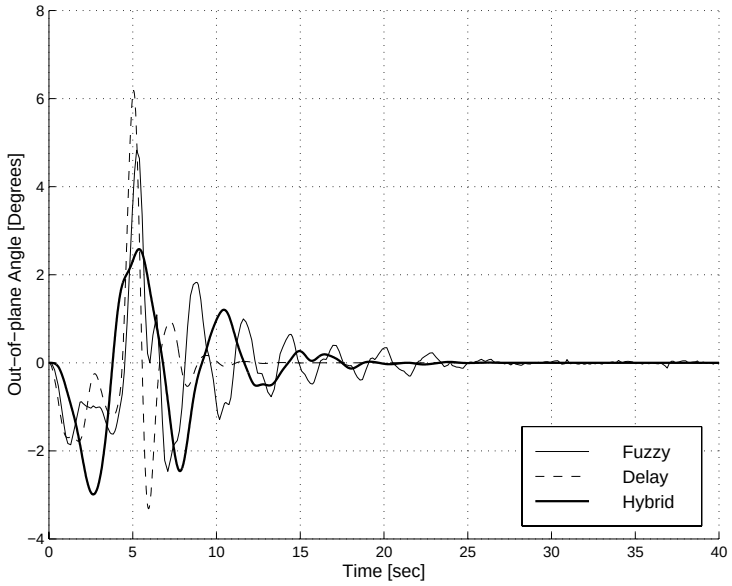

Figure 4.32: Controlled out-of-plane oscillation angle $\theta(t)$ for the compound case using the delay, fuzzy, and hybrid controllers.

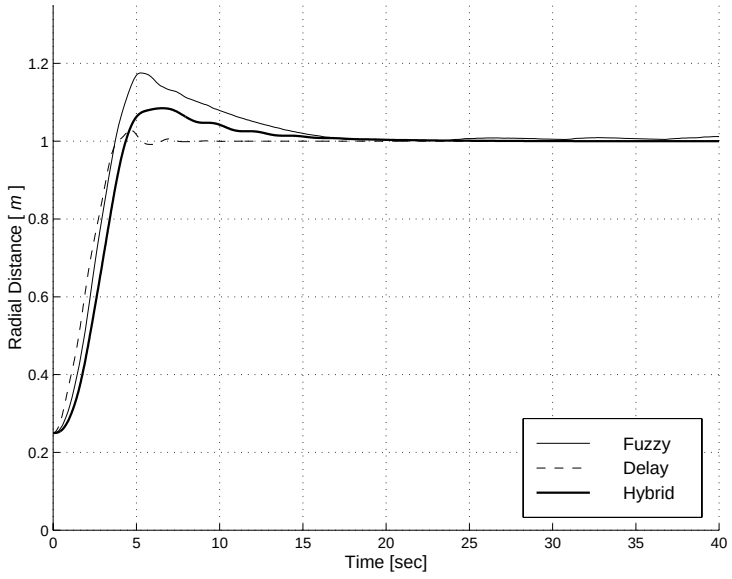

Figure 4.33: Radial distances for the compound case using the delay, fuzzy, and hybrid controllers.

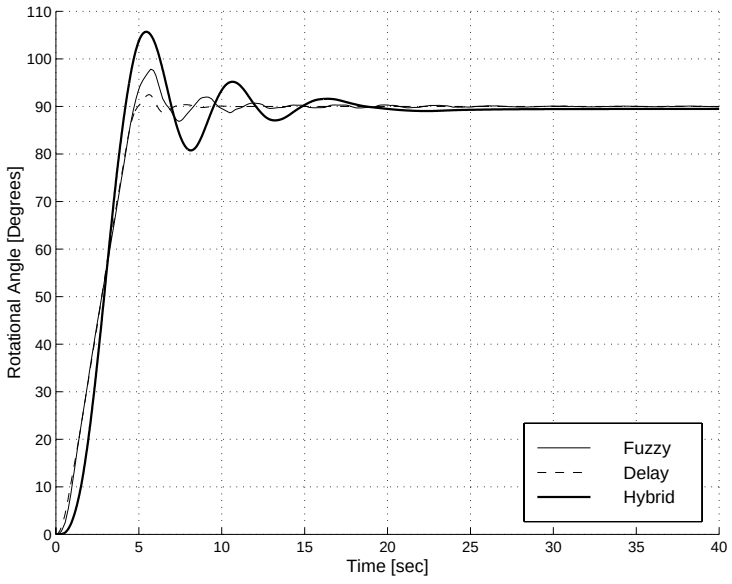

Figure 4.34: Rotational angles for the compound case using the delay, fuzzy, and hybrid controllers.

4.6.4 Damping Case

Finally, we investigate the effectiveness of the hybrid controller to damp initial disturbances. We start with an initial condition of 75° for each of the oscillation angles $\theta(t)$ and $\phi(t)$. The trolley is placed at a distance of 1.0 m on the jib to magnify the the effect of the oscillations. From Figures 4.35 and 4.36, we conclude that the hybrid controller damps this initial disturbance as fast as the delay controller, but faster than the fuzzy controller. The oscillations of the in-plane and out-of-plane angles damp in about 7 s, which is shorter than the 22 s needed by the fuzzy controller.

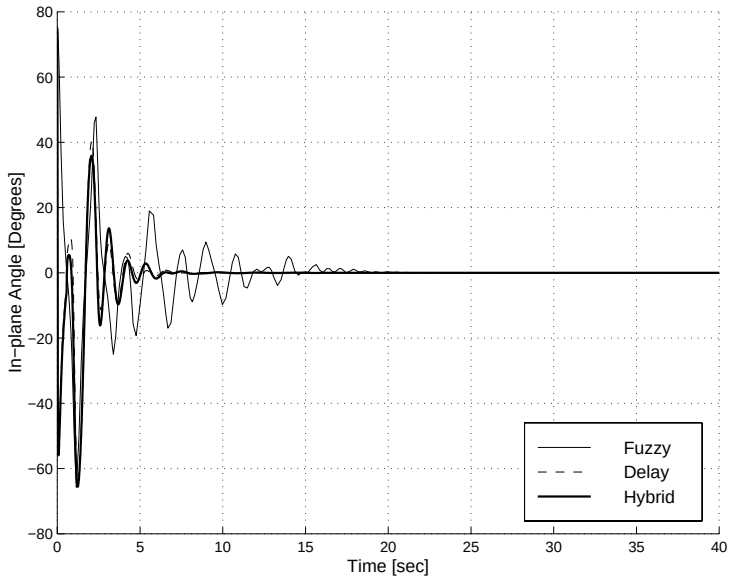

Figure 4.35: Controlled in-plane oscillation angle $\phi(t)$ for the damping case using the delay, fuzzy, and hybrid controllers.

It follows from Figures 4.37 and 4.38 that, with the hybrid controller, the control action represented by the radial and rotational deviations from the rest positions are large, as in the case of the delay controller. The maximum deviation in the radial distance is about 30 cm, which is three times that needed by the fuzzy controller and similar to that needed by the delay controller. Also the maximum oscillation of the rotational angle needed to damp the oscillations is about 27°, which is again larger than the 10° needed by the fuzzy controller. We conclude that the short time needed to damp this initial disturbance (i.e. 75°) is due to the large deviations allowed for the trolley and jib positions. This gives the fuzzy logic controller and the delay controller with low gain ($k = 0.16$) an advantage in cases where the trolley or the jib can not be moved as fast and large and the damping time is not of great importance. On the other hand, when the damping time is more important, the delay controller with high gain ($k = 0.4$) has an advantage in the sense that it results in deviations similar to those of the hybrid controller and takes shorter time to reach the end point than the hybrid controller.

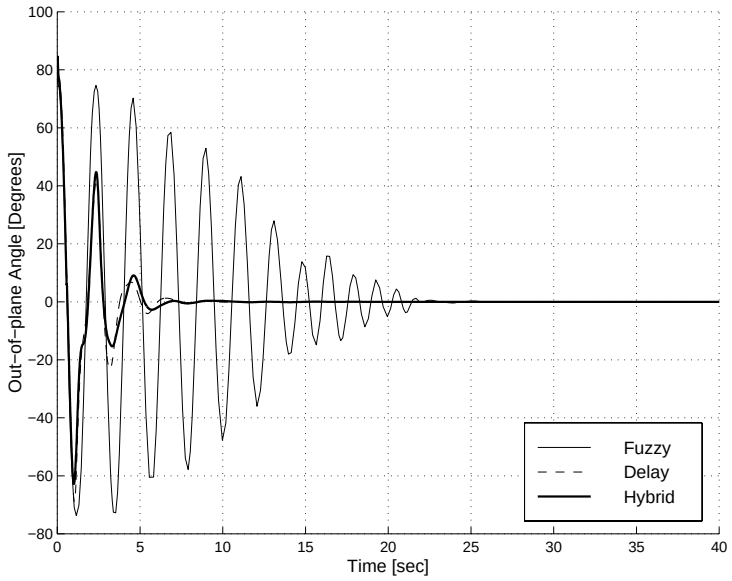

Figure 4.36: Controlled out-of-plane oscillation angle $\theta(t)$ for the damping case using the delay, fuzzy, and hybrid controllers.

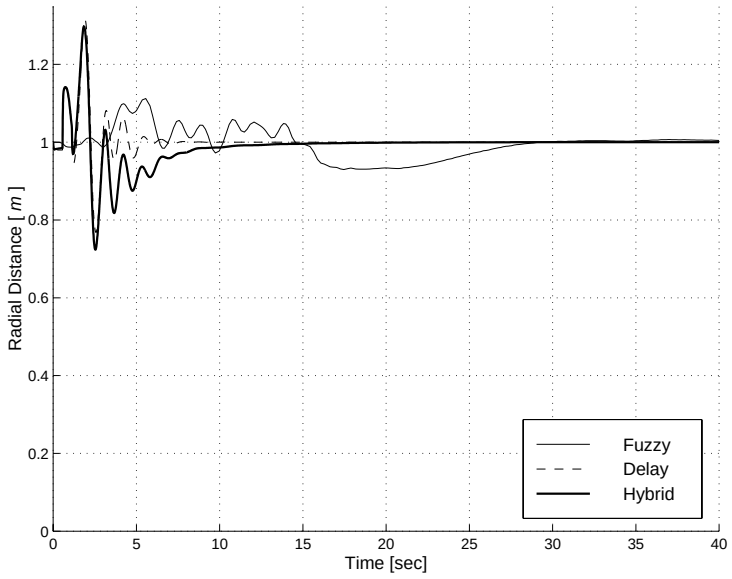

Figure 4.37: Radial distances for the damping case using the delay, fuzzy, and hybrid controllers.

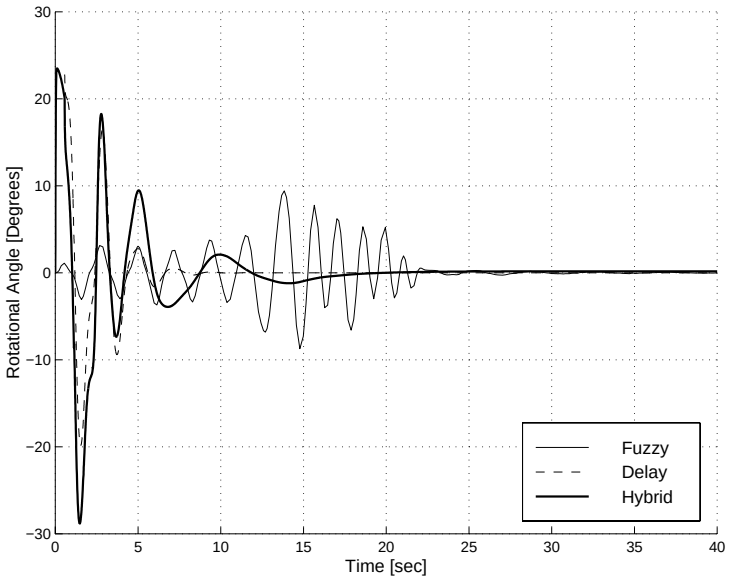

Figure 4.38: Rotational angles for the damping case using the delay, fuzzy, and hybrid controllers.

Chapter 5

Experimental Testing

To verify the numerical simulations, we built a model of a rotary crane. This chapter describes the experimental setup and the results obtained using the delay controller.

5.1 Experimental Setup

As shown in Figure 5.1, a Personal Computer is used to control the crane through an Input/Output (I/O) interface board. The I/O board in turn sends the output signals to the actuators, which move the crane. Moreover, a set of encoders and limit switches feedback information to the PC.

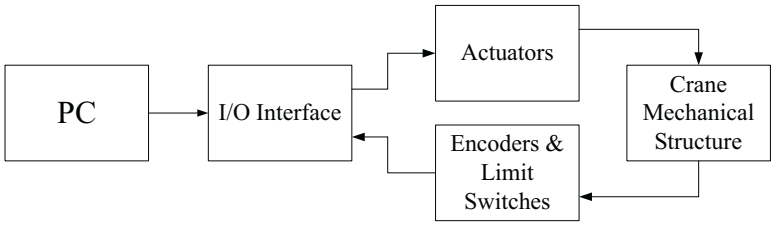

Figure 5.1: Experimental setup block diagram.

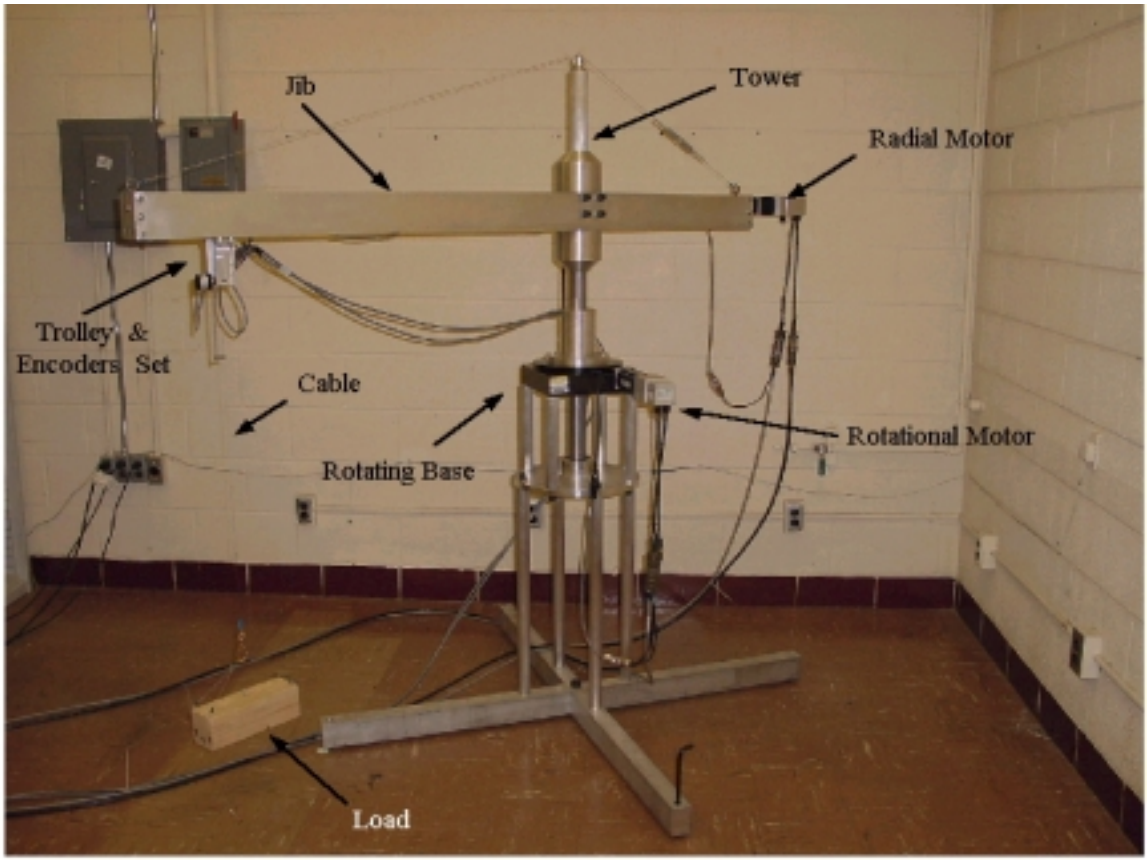

Figure 5.2: Picture of the crane model.

Figure 5.2 shows the crane model. A servomotor is connected to a rotating base, which rotates the tower of the crane. A second servomotor is connected to a gear box that drives a ball screw, which moves the trolley along the jib. A set of optical encoders are mounted on the trolley to measure the in-plane and out-of-plane angles of the payload cable. The motors used are brushless type servomotors with internal brakes. Both servomotors are equipped with internal optical encoders to read the motions of the motors. An electric circuit was designed and built to activate the servomotor brakes, Figure 5.3. Also two amplifiers are needed to drive the servomotors, thereby providing them with the required power and taking care of the communication between the motors and the control computer.

Since the brakes operate at 24V and we can not get this voltage from the interface board, we used an external power supply and two DAC to provide the 24V to the brakes. Whenever one of the motors is required to start, 9V are sent via the DAC to the relay, which in turn connects the 24V to the magnetic brakes of the motor, Figure 5.3.

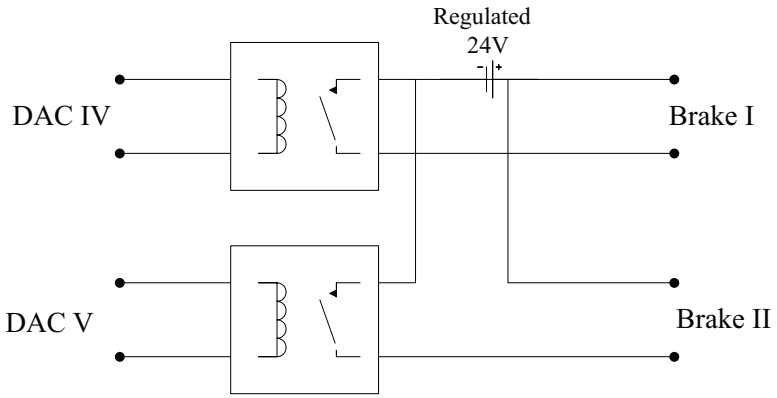

Figure 5.3: Brakes circuit.

To provide regulated voltage for the brakes and the encoders, we built two circuits to generate regulated +5V for the encoders and 24 V to the brakes, Figures 5.4 and 5.5.

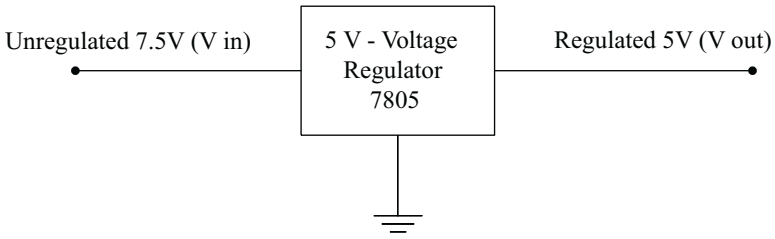

Figure 5.4: Five-volt regulation circuit.

5.1.1 I/O Interface

As explained earlier, an interface board connects the computer to the actuators (motors), encoders, etc. The interface board is the ISA Bus Servo I/O card-model 2 [15]. The main advantages of this board are its low cost and flexibility of use. The board is capable of controlling 8 motors simultaneously using an ISA-bus from any IBM compatible PC. Below is a description of the main features of the board, Figure 5.6.

Encoder Inputs: The board can handle up to 8 channels of quadrature encoder inputs. It reads phases A and B along with the index pulse Z, which is sometimes referred to as I. The counters used have 24-bit resolution. Four of these channels have been used, two for the internal encoders of the motors and two for the optical encoders of the oscillations angles.

Analog Inputs: The board has 8 channels of analog inputs, which have 13-bit resolution. The board can be configured such that the analog voltage range is either (-5/+5V) or (-10/+10V). Also the input signals can be either single-ended or differential, depending on the application.

Analog Outputs: Similar to the analog inputs, there are 8 output channels. The output voltage can be set between -10V and +10V, with a 13-bit resolution. Two DACs are used to send the voltage signal to the amplifiers. Also because of their capabilities of providing higher current than the digital I/O, two other DACs are used to control the brake relays in the brake circuits.

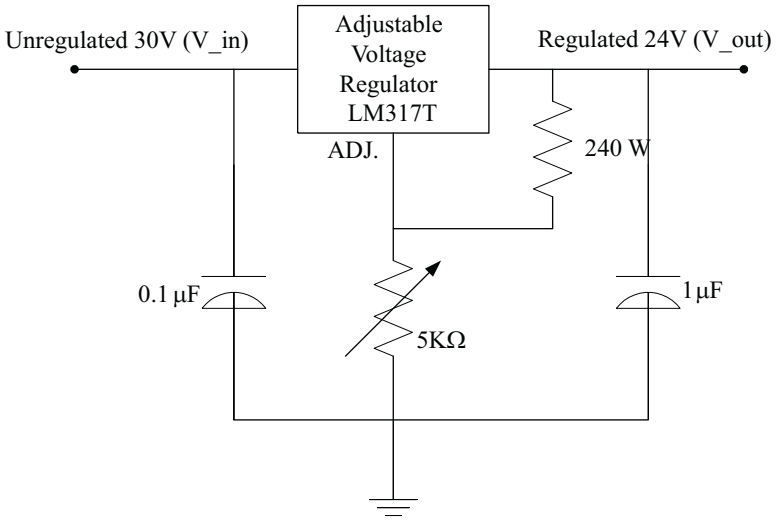

Figure 5.5: 24 volts regulation circuit.

Digital Inputs and Outputs: These are four 8-bit ports that can be configured in many ways as inputs or outputs. These ports are opto-22 compatible. Two digital outputs are used as enable signals to the amplifiers. Three other digital inputs are dedicated for a home switch of the rotating base and two limit switches on the jib.

Interval Timers: The timer interval can be programmed up to 10 minutes in increments of 25 microseconds. Also it is capable of interrupting the PC whenever the timer expires.

Battery Backup Input: It is used to maintain encoder-counting capability in event of a power failure.

Watchdog Timer: This timer is set to trap errors that might occur in the application, so if something goes wrong and the watchdog timer is not reset, then a shut down procedure will be applied. The parameters of the board can be accessed using a set of registers, which are located in the I/O space occupied by the board. The board has its connection to the outside world via four 50-pin connectors.

Figure 5.6 shows a schematic diagram of the interconnections between the interface board and the equipment attached to it.

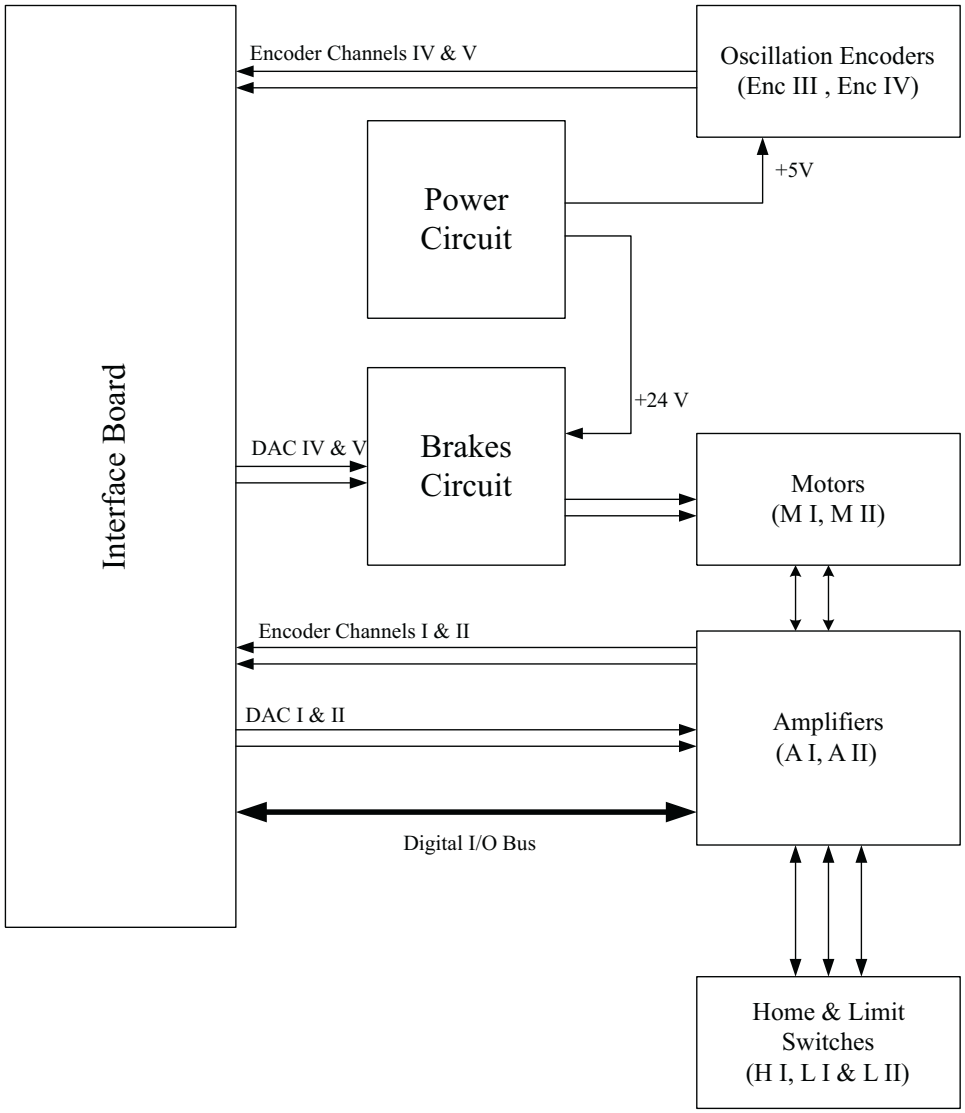

Figure 5.6: I/O interface connections.

5.2 Experimental Results

To verify the simulation results, we perform similar experiments on the actual model of the crane. The experimental parameters are very close to those used in the simulation. A factor that could cause a difference between the experiment and the simulation is friction because no friction is introduced in the simulation. Next, we present the results.

5.2.1 Radial Case (Gantry Case)

The experimental results for the radial case turned to be very close to the simulation results. Comparing the experimentally and theoretically obtained uncontrolled responses, we note that the experimentally obtained response damps with time unlike the simulations. This is the result of friction that reduces the oscillations. The controlled in-plane angle $\phi(t)$ has a peak of less than 3°, Figure 5.7. The dark line is due to noise that affects the readings of the sensors. We note that the oscillations almost vanish after 10 s. The controller has no effect on either the rotational angle $\gamma(t)$ or the out-of-plane oscillation angle $\theta(t)$. The experiment shows the feasibility of using the delay controller in damping the oscillations. Figure 5.8 shows both the desired position of the trolley set by the operator and the actual position of the trolley. We note that the overshoot is very small, about 2 cm, and the steady-state error is equal to zero.

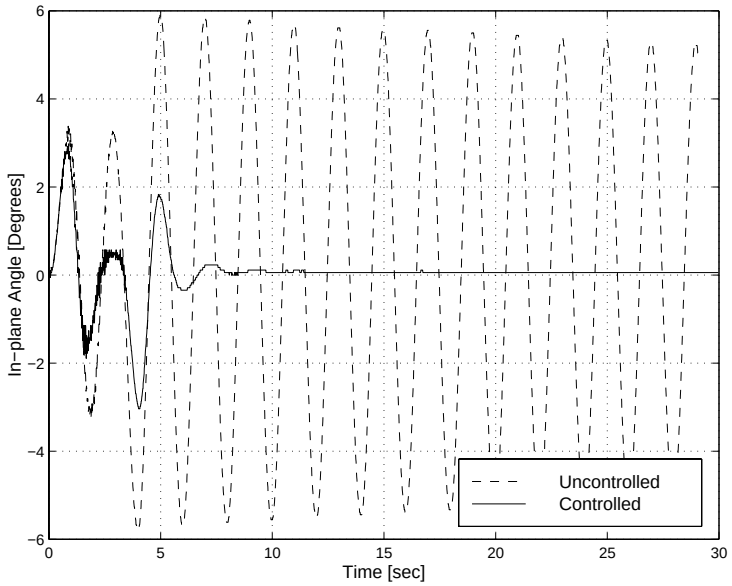

Figure 5.7: Experimentally obtained uncontrolled and controlled in-plane oscillation angle $\phi(t)$ for the gantry case using the delay controller.

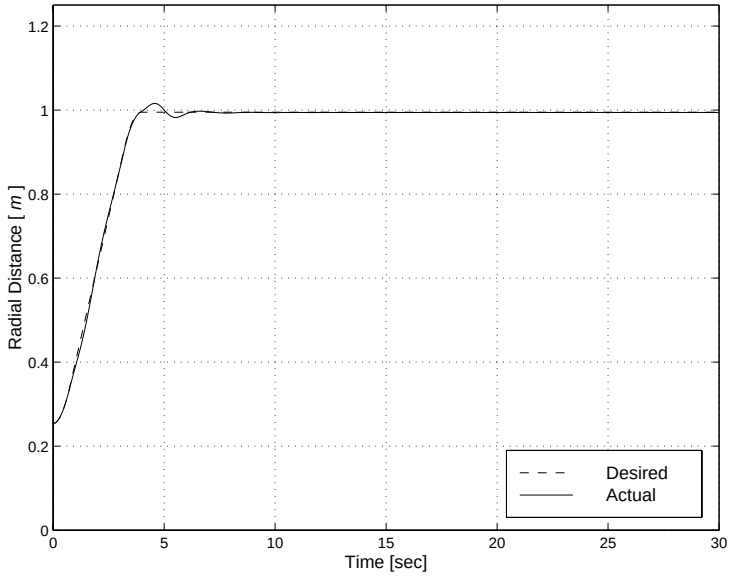

Figure 5.8: Experimentally obtained desired and actual radial distances for a gantry case using the delay controller.

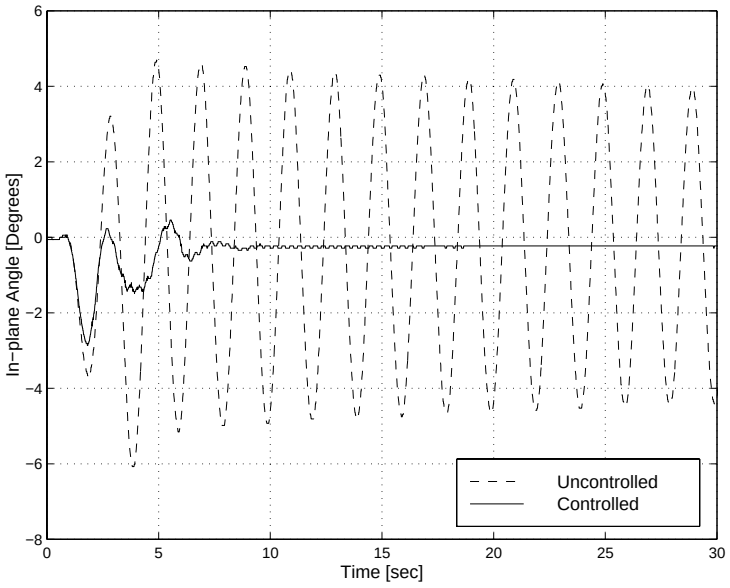

Figure 5.9: Experimentally obtained uncontrolled and controlled in-plane oscillation angle $\phi(t)$ for the rotational case using the delay controller.

5.2.2 Rotational Case

As in the simulations, the trolley is fixed at a radius of about 1.0 m and the jib is rotated 90° from its position. The uncontrolled in-plane angle $\phi(t)$, Figure 5.9, reaches close to 6°, as in the simulation results. However, the experimentally obtained uncontrolled response of the in-plane angle decays slowly with time due to friction, compared with that obtained with the simulations. The uncontrolled out-of-plane angle $\theta(t)$, Figure 5.10, reaches about $-4.5°$ during the acceleration phase and 5° during the deceleration phase. The influence of friction is also obvious in the experimentally obtained uncontrolled out-of-plane angle, which decays slowly, in contrast with the simulation results. It is clear from Figures 5.9 and 5.10 that there is a steady-state error in the oscillation angles. This error is in fact a sensor error because the load can not maintain such oscillation angles under the influence of gravity. We see from Figures 5.11 and 5.12 that it takes about 10 s to reach the final state and to reduce the oscillation angles almost to zero. The trolley here is set at a distance of about

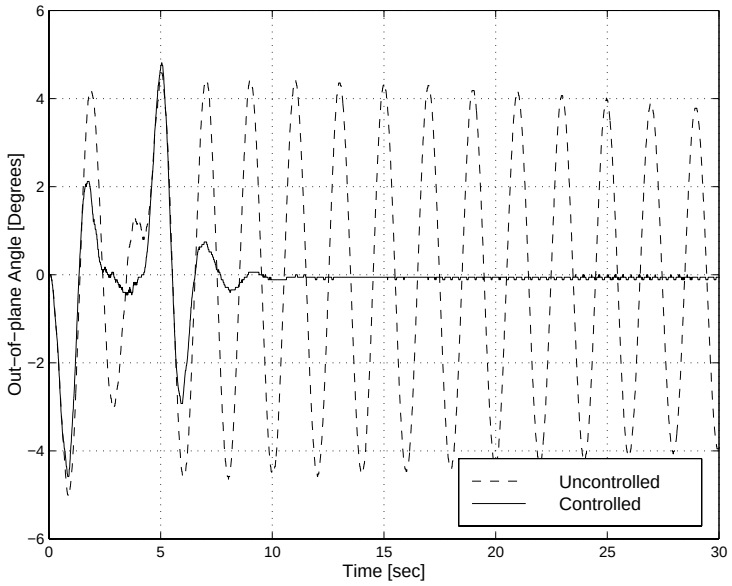

Figure 5.10: Experimentally obtained uncontrolled and controlled out-of-plane oscillation angle $\theta(t)$ for the rotational case using the delay controller.

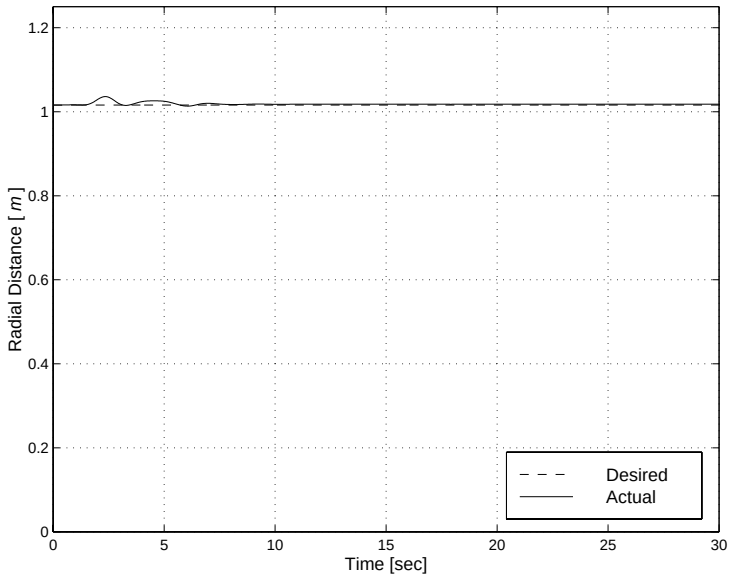

Figure 5.11: Experimentally obtained desired and actual radial distances for the rotational case using the delay controller.

1.02 m from the center. The trolley has deviated only about 2 cm from its rest position. As expected, the rotational angle of the jib has experienced a small overshoot also, only about 3°. We note the closeness of the actual rotational angle to the angle desired by the operator. This smooth tracking eases the operator manipulation of the crane.

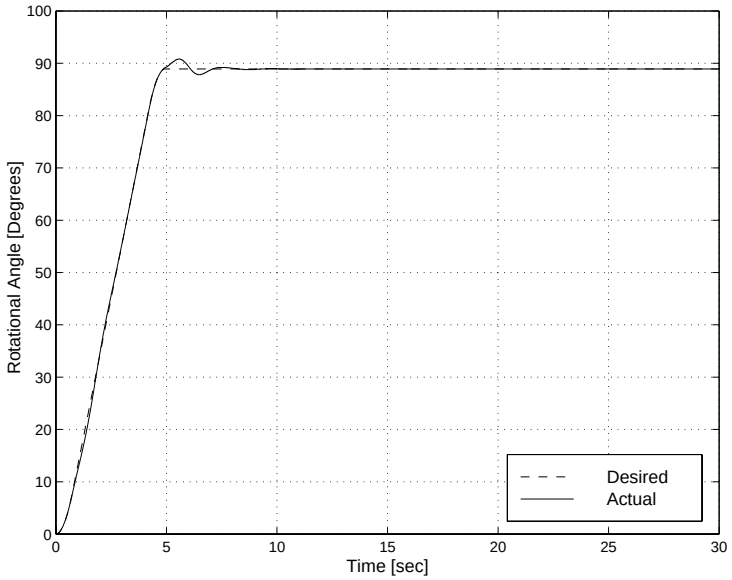

Figure 5.12: Experimentally obtained desired and actual rotational angles for the rotational case using the delay controller.

5.2.3 Compound Case

In this case, a combination of the radial and rotational motions is applied. The trolley is moved on the jib a distance of 0.77 m as in the radial case, while the jib is rotated 90° around the tower as in the rotational case.

Comparing the experimentally obtained uncontrolled in-plane and out-of-plane angles, Figures 5.13 and 5.14, with these obtained theoretically, Figures 4.12 and 4.13, we note that the energy is continuously being exchanged between the two modes as in the simulations, but the oscillation amplitudes are smaller than those obtained theoretically because of the

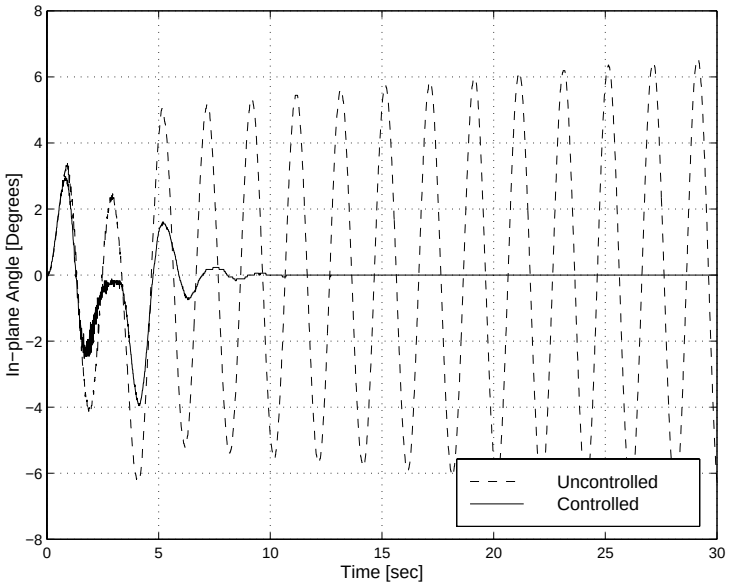

Figure 5.13: Experimentally obtained uncontrolled and controlled in-plane oscillation angle $\phi(t)$ for the compound case using the delay controller.

friction in the experiment. However, this friction is small, and consequently the oscillations persist for a long time.

As in the simulations, the controller is very effective in damping the oscillations. The in-plane angle reaches a maximum of about 3° during the acceleration phase and -4° during the deceleration phase, Figure 5.13. The oscillations are damped within 10 s. We note that some noise is affecting the readings of the encoders in the interval $(2-4\ s)$. The out-of-plane angle $\theta(t)$, Figure 5.14, reaches a maximum of approximately 6° during the deceleration phase, and it takes a slightly longer time (around 13 s) to settle down than it takes the in-plane angle. The only noticeable difference between the experiment and the simulations is that two extra seconds are needed in the experiment to damp the out-of-plane angle. Similarly, noise has affected the reading of the out-of-plane angle, which might be the reason for the difference between the experiment and the simulations. The minor remaining oscillations can be attributed to errors in the optical encoders readings.

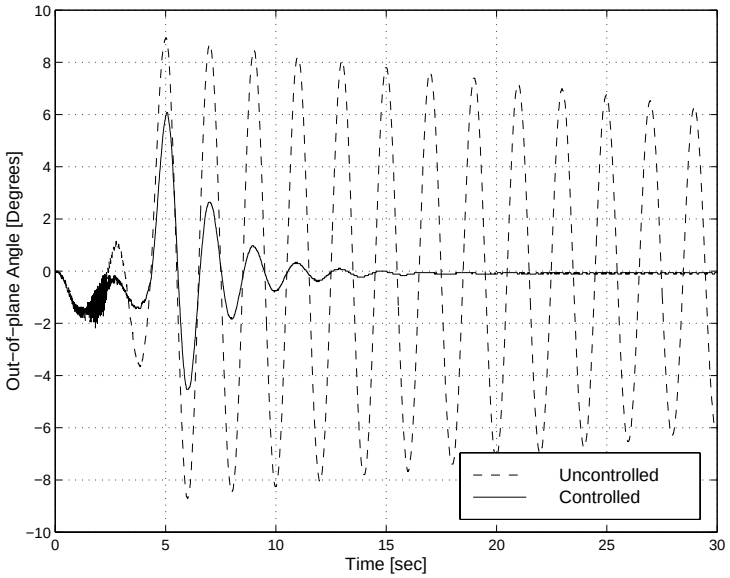

Figure 5.14: Experimentally obtained uncontrolled and controlled out-of-plane oscillation angle $\theta(t)$ for the compound case using the delay controller.

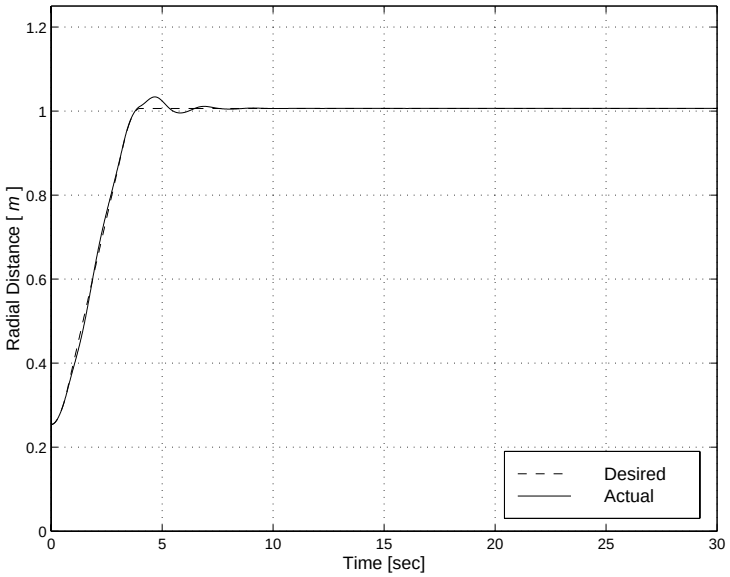

Figure 5.15: Experimentally obtained desired and actual radial distances for the compound case using the delay controller.

Figure 5.15 shows the radial distance of the trolley on the jib. The results are very similar to the simulations and the overshoot is also small (about 2 cm). With this small overshoot, the trolley takes less than 8 s to reach its end position. As for the rotational angle, Figure 5.16 shows that the overshoot is also small, about 3°. It takes about 10 s for the jib to reach its final position.

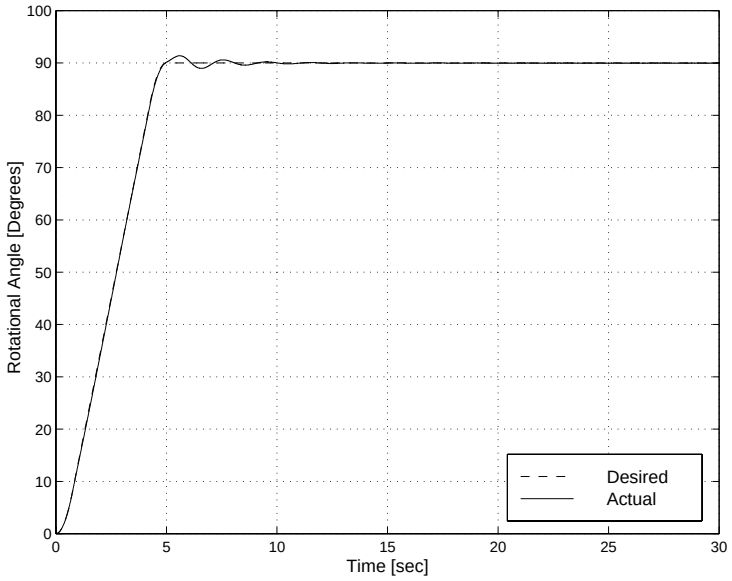

Figure 5.16: Experimentally obtained desired and actual rotational angles for the compound case using the delay controller.

5.2.4 Damping Case

Due to some constraints, the damping case performed here is different from that performed in the simulations. Here, the crane starts from the rest position and then is given an initial kick manually, which leads to a maximum in-plane angle of 9° and an out-of-plane of 11°.

It follows from Figures 5.17 that the in-plane angle takes about 8 s to be damped. It takes a similar time to damp the out-of-plane angle, Figure 5.18. The remaining minor oscillations in the oscillation angles are due to errors in the optical encoders. Figure 5.19

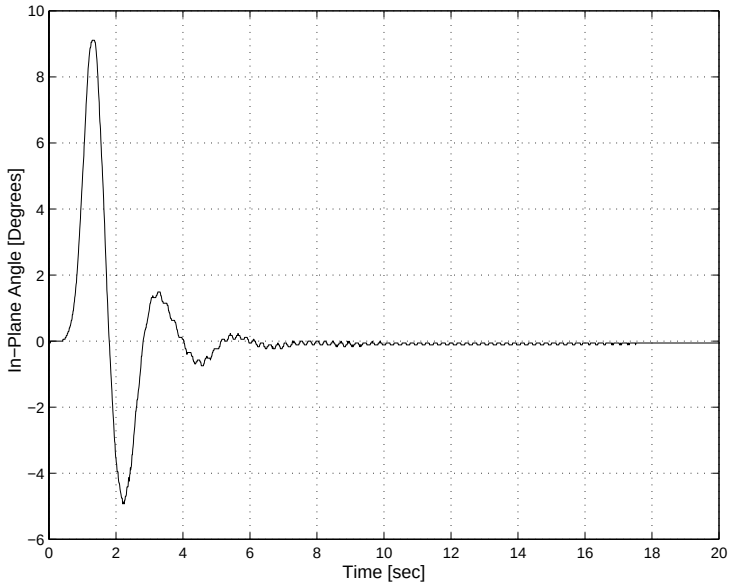

Figure 5.17: In-plane oscillation angle $\phi(t)$ for the damping case using the delay controller.

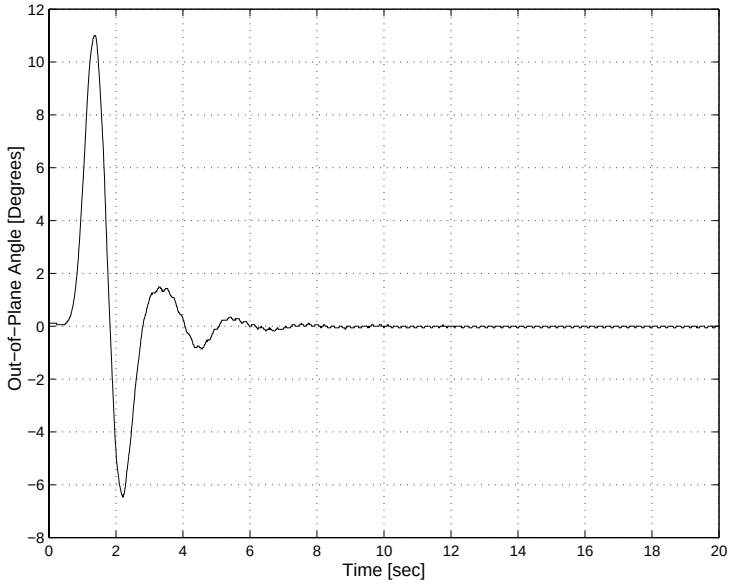

Figure 5.18: Out-of-plane oscillation angle $\theta(t)$ for the damping case using the delay controller.

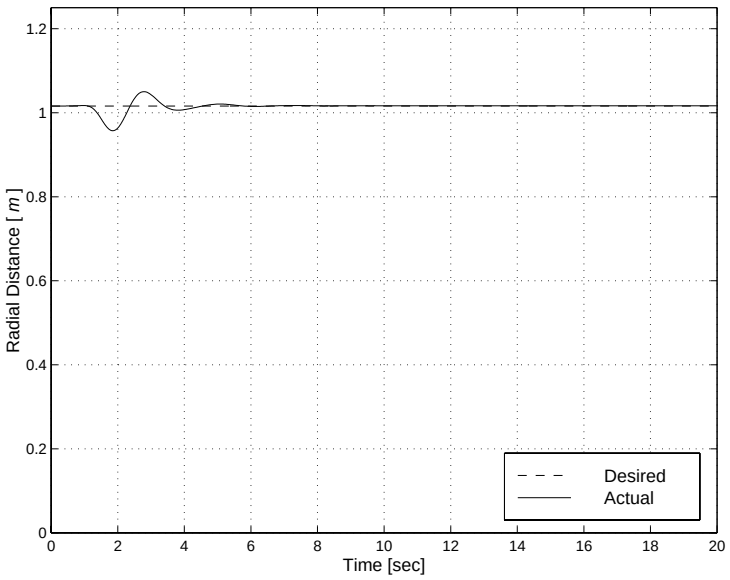

Figure 5.19: Desired and actual radial distances for the damping case using the delay controller.

shows that the maximum swing in the radial distance needed to damp the oscillations is about 4 cm. Also, Figure 5.20 shows that the maximum swing in the rotational angle needed to damp the oscillations is about 4.5°. We note that the jib takes about 8 s to settle back in the initial position, which is about 2 s higher than the time taken by the trolley to settle back in its initial position.

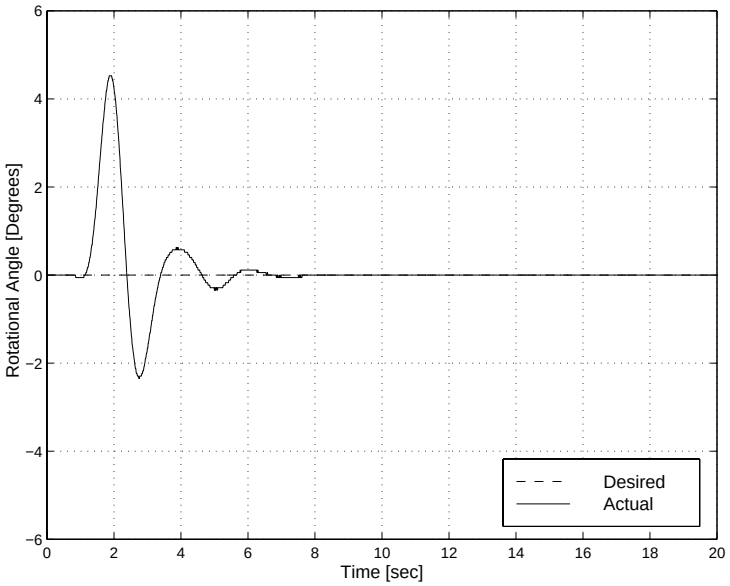

Figure 5.20: Desired and actual rotational angles for the damping case using the delay controller.

Chapter 6

Conclusion

We have derived a nonlinear model of a rotary crane, which was used later on to run several simulations for different operating conditions. Three types of controllers were designed to control the motion of the crane and reduce the payload oscillations. The first controller is a fuzzy logic controller, which uses four FIEs, two for each degree of freedom. The controller is characterized by oscillation-correction FIEs separate from those used for position tracking. After that, we introduced a delay controller, which is based on adding a feedback correction signal to the operator signal to damp the load oscillations. Finally, a hybrid of the previous two controllers was designed. The hybrid controller uses the tracking FIEs of the fuzzy controller to generate the desired position signal from the operator commands and the current position. Also, it uses the delay controller in the feedback loop to add the correction portion that takes care of damping the oscillations.

Computer simulations were run for all of the three controllers under different operating conditions. In addition to this, an experimental setup was built to verify the simulation results. When the delay controller was tested on the rotary crane model, the experimental and simulation results are in good agreement. For cases that require very larger accelerations, which might not be realizable in real life, the controller is capable of reducing the

oscillations, but it takes longer time than the simulations.

All of the controllers developed have acceptable performance, they are able to damp any oscillations that might occur during the crane movement. Still, the controllers have stability limits, which cannot be violated. As for the delay controller, the stability limits are very precise and clear. The delay controller stability is dependent on the gain k and the delay period τ. Unfortunately, this is not the case for the fuzzy controller or the hybrid controller. Their stability limits are ambiguous and not clear. So it is recommended that the fuzzy logic controller be used close to stability ranges obtained with simulations.

Even though the controllers show excellent performance, we can not pick the best controller. Depending on the application under consideration, a certain controller will be advantageous. When comparing the time it takes for the oscillation angles to decay to zero, the delay controller shows the best performance because it is the fastest in all of the cases performed.

Since the gantry crane case is a special case of the rotary crane, the results show that the hybrid controller yields the best in-plane angle oscillation. On the other hand, the delay controller yields the minimum overshoot in the radial distance of the trolley.

For rotary cranes, again the delay controller is perfect if overshoots in either the radial distance or the rotational angle are undesirable. A hybrid controller reduces the out-of-plane oscillation angles more than the fuzzy or delay controllers. As for the in-plane angle, the performance of the delay controller is comparable to those of the fuzzy and hybrid controllers. In the latter cases, the obtained in-plane angle is smaller than that obtained with the delay controller.

As mentioned earlier, the delay controller produces the fastest damping in all cases. But when large initial disturbances are present, this fast damping comes at the expense of a relatively larger overshoots in both the radial distance and the rotational angle. To overcome the large overshoots, one can reduce the gain of the delay controller. Meanwhile,

the fuzzy controller has the smallest overshoot, but at the expense of a settling time longer than that of the delay controller. The delay controller has a great advantage in its capability to work in the feedback loop along with other controllers working on the operator input in the feedforward loop.

From the previous results, if the time of the crane motion is the main factor, then the delay controller should be used. But if the oscillation angles are the concern, then the hybrid controller should be used.

Further investigations on this project need to consider the use of different membership functions in the fuzzy controller, such as Gaussian function and the modification of the rules and the structure of the rotational FIE to account for the coupling between the radial and rotational motions. Also, since the error in the radial position turned out to be small, a reduction in the range of the radial error membership function should be considered. As for the delay controller, a three-dimensional model can be developed to take advantage of the load hoisting for damping the oscillations.

Bibliography

[1] M. J. Patyra and D. M. Mlynek. Fuzzy Logic Implementation and Applications. Wiley and Teubner, Chichester, NY, 1996.

[2] N. Vadiee, M. Jamashidi, and T. J. Ross. Fuzzy Logic and Control - Software and Hardware Applications. Prentice Hall, Englewood Cliffs, NJ, 1993.

[3] K. Ogata. Modern Control Engineering. Prentice Hall, Upper Saddle River, NJ, 1997.

[4] J. E. Slotine and W. Li. Applied Nonlinear Control. Prentice Hall, Englewood Cliffs, NJ, 1991.

[5] R. J. Henry. Cargo pendulation reduction on ship-mounted cranes. Master's thesis, Virginia Polytechnic Institute and State University, 1999.

[6] Z. N. Masoud, A. H. Nayfeh, R. J. Henry, and D. T. Mook, "Cargo pendulation reduction on ship-mounted cranes via boom-luff and slew angles actuation," in Proceedings of the 41th Structures, Structural Dynamics, and Materials Conference, Atlanta, GA, AIAA-2000-1543, 2000.

[7] R. J. Henry, Z. N. Masoud, A. H. Nayfeh, and D. T. Mook, "Cargo pendulation reduction on ship-mounted cranes via boom-luff angle actuation," accepted for publication, Journal of Vibration and Control, 2000.

[8] M. J. Nally and M. B. Tarbia, "Design of a fuzzy logic controller for swing-damped transport of an overhead crane payload," in Proceedings of the ASME Dynamic Systems and Control Division, DSC-Vol. 58, pp. 389–398, 1994.

[9] A. R. Golafshani and J. D. Aplevich, "Computation of time-optimal trajectories for tower cranes," in Proceedings of the IEEE Conference on Control Applications, Albany, NY, pp. 1134–1139, 1995.

[10] G. G. Parker, B. Petterson, C. R. Dohrmann, and R. D. Robinett, "Vibration suppression of fixed-time jib crane maneuvers," in Proceedings of the SPIE Symposium on the Smart Structures and Materials Conference, Vol. 2447, pp. 131-140, 1995.

[11] G. G. Parker, B. Petterson, C. R. Dohrmann, and R. D. Robinett, "Command shaping for residual vibration free crane maneuvers," in Proceedings of the American Control Conference, Seattle, WA, pp. 934–938, 1995.

[12] G. G. Parker, R. D. Robinett, B. J. Driessen, and C. R. Dohrmann, "Operator in-the-loop control of rotary cranes," in Proceedings of the SPIE Symposium on the Smart Structures and Materials Conference, Vol. 2721, pp. 364–372, 1996.

[13] MathWorks, Inc. Version 2. Fuzzy logic toolbox for use with Matlab, 1998.

[14] MathWorks, Inc. Version 3. Simulink, dynamic system simulation for Matlab, 1999.

[15] Servo To Go, Inc. Revision 2.0. Isa bus servo I/O card, model 2 hardware manual, May 1999.

[16] G. Goebel. An introduction of fuzzy control systems. http://www.isis.ecs.soton.ac.uk/research/nfinfo/fuzzycontrol.html.

[17] Femont n.v. Belgium. Gantry crane. http://www.femont.com/noord.jpg.

[18] Tower Cranes of America, Inc. 1999.
http://www.towercranes.com/Photo-Scans/30/30-13.jpg.

Vita

Amjed Al-Mousa was born on May 11, 1977 in Amman, Jordan. In 1994, he graduated from the Islamic Educational College (high school). Then he attended the University of Jordan, where he received his Bachelor of Science degree in Electrical Engineering. In the Summer of 1999, he came to the United States where he joined Virginia Tech to work towards his Master of Science in Electrical Engineering. By the beginning of 2001, he will start working at the Silicon Valley with INTEL as a software engineer.